Enhanced representation of soil NO emissions in the Community Multi-scale Air Quality (CMAQ) model version 5.0.2

Quazi Z. Rasool[1], Rui Zhang[1], Benjamin Lash[1*], Daniel S. Cohan[1], Ellen J. Cooter[2], Jesse O. Bash[2] and Lok N. Lamsal[3,4]

[1]{Department of Civil and Environmental Engineering, Rice University, Houston, Texas, USA}

[2]{Computational Exposure Division, National Exposure Research Laboratory, Office of Research and Development, US Environmental Protection Agency, RTP, NC, USA}

[3]{Goddard Earth Sciences Technology and Research, Universities Space Research Association, Columbia, MD 21046, USA }

[4]{NASA Goddard Space Flight Center, Greenbelt, MD 20771, USA}

[*]{now at: School of Natural Sciences, University of California, Merced, CA}

Correspondence to: Daniel Cohan (cohan@rice.edu)

Abstract

Modeling of soil nitric oxide (NO) emissions is highly uncertain and may misrepresent its spatial and temporal distribution. This study builds upon a recently introduced parameterization to improve the timing and spatial distribution of soil NO emission estimates in the Community Multi-scale Air Quality (CMAQ) model. The parameterization considers soil parameters, meteorology, land use, and mineral nitrogen (N) availability to estimate NO emissions. We incorporate daily year-specific fertilizer data from the Environmental Policy Integrated Climate (EPIC) agricultural model to replace the annual generic data of the initial parameterization, and use a 12 km resolution soil biome map over the continental US. CMAQ modeling for July 2011 shows slight differences in model performance in simulating fine particulate matter and ozone from IMPROVE and CASTNET sites and NO_2 columns from Ozone Monitoring Instrument (OMI) satellite retrievals. We also simulate how the change in soil NO emissions scheme affects the expected O_3 response to projected emissions reductions.

1 Introduction

Nitrogen oxides (NO_x=NO+NO_2) play a crucial role in tropospheric chemistry. Availability of NO_x influences the oxidizing capacity of the troposphere as NO_x directly reacts with hydroxyl radicals (OH) and catalyzes tropospheric ozone (O_3) production and destruction (Seinfeld and Pandis, 2012). NO_x also affects the lifetime of reactive greenhouse gases like CH_4 by influencing its dominant oxidant OH (Steinkamp and Lawrence, 2011), thus affecting the Earth's radiative balance (IPCC, 2007). NO_x also influences rates of formation of inorganic particulate matter (PM) (Wang et al., 2013) and organic PM (Seinfeld and Pandis, 2012).

Soil NO_x emissions accounts for ~15-40 % of the tropospheric NO_2 column over the continental United States (CONUS), and up to 80% in highly N fertilized rural areas like the Sahel of Africa (Hudman et al., 2012). The estimated amount of nitric oxide (NO) emitted from soils is highly uncertain, ranging from 4-15 Tg-N yr^{-1}, with different estimates of total global NO_x budget also showing a mean difference of 60-70% (Potter et al., 1996; Davidson and Kingerlee, 1997; Yienger and Levy, 1995; Jaeglé et al., 2005; Stavrakou et al., 2008; Steinkamp and Lawrence, 2011; Miyazaki et al., 2012; Stavrakou et al., 2013; Vinken et al., 2014). Soil NO_x is mainly emitted as NO through both microbial activity (biotic/enzymatic) and chemical (abiotic/non-enzymatic) pathways, with emission rates varying as a function of meteorological conditions, physicochemical soil properties, and nitrogen (N) inputs from deposition and fertilizer or manure application (Pilegaard, 2013; Hudman et al, 2012). The fraction of soil N emitted as NO varies with meteorological and soil conditions such as temperature, soil moisture content, and pH (Ludwig et al., 2001; Parton et al., 2001; van Dijk et al., 2002; Stehfest and Bouwman, 2006).

Different biome types, comprised of vegetation and soil assemblages exhibit different NO emission factors under different soil conditions and climate zones. One of the early attempts to stratify soil NO based on different biomes by Davidson and Kingerlee (1997) involved compiling over 60 articles and 100 field estimates. They clearly identified biomes associated with low NO emissions like swamps, tundra, and temperate forests, and those with high soil NO fluxes like tropical savanna/woodland and cultivated agriculture. For instance, high soil NO fluxes were observed in croplands, savannahs or woodlands, N-rich temperate forests and even boreal/tropical forests with low NO_2^- availability in warm conditions and acidic soil (Kesik et al., 2006; Cheng et al., 2007; Su et al., 2011). This approach, however, fails to capture within-

biome variation in NO emissions (Miyazaki et al., 2012; Vinken et al., 2014). For example, mature forests give higher soil NO flux than rehabilitated and disturbed ones due to higher initial soil N (Zhang et al., 2008). Steinkamp and Lawrence (2011) more recently compiled worldwide emission factors from a dataset consisting of 112 articles with 583 field measurements of soil NO_x covering the period from 1976 to 2010, and regrouped them into 24 soil biome type based on MODIS land cover category as well as Köppen climate zone classifications (Kottek et al., 2006).

Both wet and dry deposition act as sources of nitrogen to soils (Yienger and Levy, 1995; Hudman et al., 2012). N is deposited in both oxidized (e.g., nitrate) and reduced (e.g., ammonium) forms, with ammonium representing a growing share of N deposition in the U.S. as anthropogenic NO_x emissions are controlled (Li et al., 2016).

Fertilizer (organic and inorganic) application represent controllable influences on soil N emissions (Pilegaard, 2013) and are leading sources of reactive nitrogen (N) worldwide (Galloway and Cowling, 2002). U.S. fertilizer use increased by nearly a factor of 4 from 1961 to 1999 (IFIA, 2001). Soil NO emissions increase with rising fertilizer application, with conversion rate of applied fertilizer N to NO_x being up to ~ 11% (Williams et al., 1988; Shepherd et al., 1991). Open and closed chamber studies have shown increasing fertilizer application to increase both NO and N_2O fluxes simultaneously, but with variability in NO/N_2O emission ratio (Harrison et al., 1995; Conrad, 1996; Veldkamp and Keller, 1997).

Meteorological conditions influence soil NO emission rates.() Soil NO pulsing events occur when water stressed nitrifying bacteria, which remain dormant during dry periods, are activated by the first rains and start metabolizing accumulated N in the soil. Large pulses of biogenic NO emissions of up to 10–100 times background levels often follow the onset of rain after a dry period and can last for 1–2 days (Davidson, 1992; Yienger and Levy, 1995; Scholes et al., 1997; Jaeglé et al., 2004; Hudman et al., 2010; Hudman et al., 2012; Zörner et al., 2016).

Adsorption onto plant canopy surfaces can reduce the amount of soil NO emissions entering the broader atmosphere. Yienger and Levy (1995) (YL) soil NO scheme followed a Canopy Reduction Factor (CRF) approach (Wang et al., 1998) to account for the reduction of soil NO emission flux *via* stomatal or cuticle exchange as a function of dry deposition within the canopy on a global scale.

Contemporary air quality models such as the Community Multi-scale Air Quality (CMAQ) model most often use an adaptation of the YL scheme to quantify soil NO emissions as a function of fertilizer application, soil moisture, precipitation and CRF (Byun and Schere, 2006). However, YL has been found to underestimate emissions rates inferred from satellite and ground measurements by a factor ranging from 1.5 to 4.5, and to misrepresent some key spatial and temporal features of emissions (Jaeglé et al., 2005; Wang et al., 2007; Boersma et al., 2008; Zhao and Wang, 2009; Lin, 2012; Hudman et al., 2012; Vinken et al., 2014). This overall underestimation can be attributed to several uncertainties in the modeling settings, such as inaccurate emissions coefficients, poor soil moisture data, deriving soil temperatures from ground air temperatures, neglecting nitrogen deposition and outdated fertilizer application rates (Yienger and Levy, 1995; Jaeglé et al., 2005; Delon et al., 2007; Wang et al., 2007; Boersma et al., 2008; Delon et al., 2008; Hudman et al., 2010; Steinkamp and Lawrence, 2011; Hudman et al., 2012).

The Berkley Dalhousie Soil NO Parameterization (BDSNP) scheme, originally implemented by Hudman et al. (2012) in the GEOS-Chem global chemical transport model, outperforms YL by better representing biome type, the timing of emissions, and actual soil temperature and moisture (Hudman et al., 2010).

We implement BDSNP in CMAQ by using the Environmental Policy Integrated Climate (EPIC) biogeochemical model for dynamic representation of the soil N pool on a day-to-day basis. EPIC is a field-scale biogeochemical process model developed by the United States Department of Agriculture (USDA) to represent plant growth, soil hydrology, and soil heat budgets for multiple soil layers of variable thickness, multiple vegetative systems and crop management practices (Cooter et al., 2012). EPIC can model up to 1 sq. km (100 ha) spatially and on a daily time scale (CMAS, 2015). EPIC simulations are compatible with spatial and temporal scale of CMAQ as well (Bash et al., 2013). EPIC accounts for different agricultural management scenarios, accurate simulation of soil conditions and plant growth to produce plan demand-driven fertilizer estimates for BDSNP (Cooter et al., 2012; Bash et al., 2013).

Baseline soil NO emission rate for each location (Hudman et al., 2012; Vinken et al., 2014), use a new soil biome map with finer-scale representation of land cover systems consistent with

typical resolution of a regional model. We also built an offline version of BDSNP, which can use benchmarked inputs from the CMAQ and allows quick diagnostic based on soil NO estimates for sensitivity analysis (Supplementary material Section S.2).

2 Methodology

2.1 Implementation of advanced soil NO parameterization in CMAQ

2.1.1 Land surface model (LSM)

Our implementation of the BDSNP soil NO parameterization in CMAQ uses Pleim-Xiu Land Surface Model (Pleim and Xiu, 2003). Compared to the coarser LSM in GEOS-Chem (Bey et al., 2001), Pleim-Xiu provides finer-scale estimates of soil moisture and soil temperature based on solar radiation, temperature, Leaf Area Index (LAI), vegetation coverage, and aerodynamic resistance. The rich amount of information available from the Pleim-Xiu LSM enables refined representation of soil moisture and soil temperature for implementation in soil NO parameterization.

2.1.2 Canopy reduction factor

The original implementation of BDSNP in GEOS-Chem did not provide specific spatial-temporal variation of CRF in each modeling grid, but used a monthly average CRF from Wang et al. (1998). Wang et al. (1998) included an updated CRF as part of their implementation of YL into GEOS-Chem. This CRF is based on wind speed, turbulence, canopy structure, deposition constants, and other physical variables. In the GEOS-Chem implementation of BDSNP, this CRF reduced the flux by ~ 16%, from 10.7 Tg-N yr^{-1} above soil to 9 Tg-N yr^{-1} above canopy (Hudman et al., 2012).

Our BDSNP implementation for CMAQ uses the same approach of integrating CRF as used in Wang et al. (1998) with the biome categorization based on Steinkamp and Lawrence (2011) and Köppen climate classes (Kottek et al. 2006) in the soil NO_x parametrization itself.

2.1.3 Fertilizer

YL in CMAQ assumed a linear correlation between fertilizer application and its induced emissions over general growing season, May-August in the Northern Hemisphere and November-February in the Southern Hemisphere (Yienger and Levy, 1995) rather than peaking near the time of fertilization at the beginning of the local growing season. This likely caused inaccurate temporal representation of fertilizer driven emissions in certain regions (Hudman et al., 2012). The GEOS-Chem implementation of BDSNP applied a long-term average fertilizer application with a decay term after fertilizer is applied. Constant fertilizer emissions neglect an important phenomenon: applying fertilizer during a dry period when neither plants nor bacteria may have the water available to use it may result in a large pulse when the soil is eventually re-wetted (Pilegaard, 2013). Such dry spring N fertilizer application is common practice in the mid-west and southern plains in the U.S. (Cooter et al., 2012). The current fertilizer data used for the BDSNP is scaled to global 2006 emissions by Hudman et al. (2012) using a spatial distribution for year 2000 from Potter et al. (2010). This global database reported by Potter et al. (2010) is already 8 years out of date in magnitude and 14 years out of date for relative distribution, and has relatively coarse resolution based on out-of-date long term average (national-level fertilizer data from 1994 to 2001). Using recent fertilizer application information is essential to soil NO estimates given the fact that N fertilizer is the major contributor to plant nutrient use in US, and its share has been increasing from 11,535,000 short tons in 2001 to 12,840,000 short tons in 2013 (USDA ERS, 2013). Our implementation of BDSNP into CMAQ is designed to enable updates by subsequent developers to use new year- and location- specific fertilizer data. We use the Fertilizer Emission Scenario Tool for CMAQ (FEST-C v1.1, http://www.cmascenter.org) to incorporate EPIC simulations for 2011 into our CMAQ runs. Land use and management practices (type and timing of farm practices such as tillage) in EPIC are updated annually based on the USDA Agricultural Resource Management Survey (ARMS) (Cooter et al., 2012).

2.1.4 N Deposition

YL in CMAQ neglects nitrogen deposition, which can result in a 0.5 Tg/yr underestimation in soil NO_x globally (~5%) (Hudman et al., 2012). The current implementation of the EPIC model in FEST-C inputs oxidized and reduced form of N deposition directly into soil nitrate and ammonium pools each day. In our implementation of BDSNP, these daily time series derive from previous CMAQ simulation. Inclusion of this deposition N source reduces the simulated plant-based demand for additional N fertilizer applications. This reduced fertilizer demand due to additional deposition source is based on the theoretical plant nutrient cycle and is implicit to how actual farming practices are applied in EPIC. The bi-directional exchange capability of CMAQ is also included, but currently it affects the ammonium pool only (Bash et al., 2013).

2.1.5 Formulation of soil NO scheme

Figure 1 provides the flow chart of the BDSNP scheme implementation, which has the option to run in-line with CMAQ, or as an offline emissions parameterization. Static input files in Hudman et al. 2012 BDSNP implementation (labelled as 'old' in Fig. 1) such as those giving soil biome type with climate zone and global fertilizer pool are needed to determine the soil base emission value at each modeling grid. The Meteorology-Chemistry Interface Processor (MCIP) (Otte and Pleim, 2010) takes outputs from a meteorological model such as Weather Research and Forecasting (WRF) model (Skamarock et al., 2008) to provide a complete set of meteorological data needed for emissions and air quality simulations.

There are seven key input environment variables and two key output environment variables in our implementation of BDSNP. Table S1 lists their names and corresponding functionalities.

Our implementation of the BDSNP soil NOx emission, S_{NO_x} in CMAQ multiplies a base emission factor (A) by scaling factors dependent on soil temperature (T) and soil moisture (θ), i.e., $f(T)$, $g(\theta)$ and a pulsing term (P) (equation 1). The base emission factor depends on biome type under wet or dry soil conditions. The pulsing term depends on the length of the dry period, rather than the accumulated rainfall amount considered by YL. The CRF term estimate the fractional reduction in soil NO_x flux due to canopy resistance.

198 $S_{NO_x}\, Flux(\frac{ng\ N}{m^2 s}) =$

199 $A'_{biome}(N_{avail}) \times f(T) \times g(\theta) \times P(l_{dry}) \times CRF(LAI, Meterology, Biome)$ (1)

200 $A'_{biome} = A_{biome} + N_{avail} \times \bar{E}$ (2)

201 $N_{avail}(t) = N_{avail\ Fert}(0) \times e^{-\frac{t}{\tau_1}} + F \times \tau_1 \times \left(1 - e^{-\frac{t}{\tau_1}}\right) + N_{avail\ Dep}(0) \times e^{-\frac{t}{\tau_2}} + D \times \tau_2 \times$

202 $(1 - e^{-\frac{t}{\tau_2}})$

203 (3)

204 Fertilizer and deposition both contribute to modifying the A'_{biome} emissions coefficients for each
205 biome. Available nitrogen (N_{avail}) at time *t* from fertilizer and deposition is multiplied by
206 emission rate, $\bar{E}$, based on the observed global estimates of fertilizer emissions (~ 1.8 Tg-N yr^{-1})
207 by Stehfest and Bouwman (2006) and added to biome specific soil NO emission factors (A_{biome})
208 from Steinkamp and Lawrence (2011) to give the net base emission factor (A'_{biome}) (Eq. (2) and
209 Eq. (3)). The resulting A' is multiplied by the meteorological scaling or response factors: $f(T)$,
210 $g(\theta)$, and $P(l_{dry})$ as in Eq. (1). The soil temperature response or scaling factor $f(T)$ is simplified to
211 be exponential everywhere. NO flux now depends on soil moisture (θ) instead of rainfall, and it
212 increases smoothly to a maximum value before decreasing as the ground becomes water
213 saturated. In Eq. (3), *F* is fertilization rate (kg ha^{-1}), *D* is the wet and dry deposition rate (kg ha^{-1})
214 considered as an additional fertilization rate, and τ is decay time, which is 4 months for fertilizer
215 (τ_1) and 6 months for deposition (τ_2) (Hudman et al. 2012).

216 BDSNP uses a Poisson function to represent the dependence of emission rates on soil moisture
217 (θ), where the parameters '*a*' and '*b*' vary for different climates such that the maximum of the
218 function occurs at $\theta = 0.2$ for arid soils and $\theta = 0.3$ otherwise (Hudman et al. 2012). We adopt
219 the same approach in CMAQ, as follows:

220 $f(T) * g(\theta) = e^{0.103*T} * a * \theta * e^{-b*\theta^2}$ (4)

221 The pulsing term depends on the length of the dry period (l_{dry}) and a change in soil moisture
222 instead of on the amount of precipitation (Hudman et al., 2012).

The pulsing term for emissions when rain follows a dry period is

$$P(l_{dry}, t) = [13.01 * \ln(l_{dry}) - 53.6] * e^{-c*t} \quad (5)$$

In this equation, l_{dry} is the length of the dry period that preceded the rain and c = 0.068 hour^{-1} defines the exponential decay of the pulse.

Beyond this basic implementation of the above stated BDSNP framework into CMAQ, there were major modifications (highlighted as 'new' in Fig. 1) in the form of: a) updating biome map consistent with CMAQ, b) incorporating year- and location- specific fertilizer data using EPIC outputs and c) development of an offline BDSNP module. Our work focuses on those developments discussed in detail in the sections to follow.

2.2 Soil biome map over CONUS

The original implementation of BDSNP used the global soil biome data from the GEOS-Chem, with emission factors for each biome under dry/wet conditions taken from Steinkamp and Lawrence (2011) (Appendix Table A1). Our implementation in CMAQ uses a finer resolution (12 km) soil biome map over CONUS. The map is generated from the 30-arc-second (approximately 1 kilometer) NLCD40 (National Land Cover Dataset) for 2006, with 40 land cover/land use classifications. A mapping algorithm table (see Appendix Table A2) was created to connect the land use category to soil biome type (Table A1) based on best available knowledge. For the categories with identical names, such as 'evergreen needleleaf forest', 'deciduous needleleaf forest', 'mixed forest', 'savannas' and 'grassland', the mapping is direct. Categories in NLCD40, which are subsets of the corresponding biome category, are consolidated into one category by addition. For example, 'permanent snow and ice' and 'perennial ice-snow' in NLCD40 are combined to form 'snow and ice'; 'developed open space', 'developed low intensity', 'developed medium intensity', and 'developed high intensity' are added to form 'urban and built-up lands'. For the categories appearing only in NLCD40, the mapping algorithm is determined by referring to the CMAQ mapping scheme, available in Cross-Section and Quantum Yield (CSQY) data files in the CMAQ coding. One such case is to map 'lichens' and

250 'moss' in NLCD40 to the category 'grassland' in soil biome. Furthermore, a model resolution
251 compatible Köppen climate zone classification (Kottek et al., 2006) was added to allocate
252 different emission factor for the same biome type e.g. to account for different altitudes of
253 'grassland' at different locations. There are five climate zone classifications, namely A:
254 equatorial, B: arid, C: warm temperature, D: snow, E: polar. A 12 km CONUS model resolution
255 climate zone classification map (see Figure 2) was created using the Spatial Allocator based on
256 the county level climate zone definition as the surrogate based on a dominant land use,
257 (http://koeppen-geiger.vu-wien.ac.at/data/KoeppenGeiger.UScounty.txt).

258 Figure 2 compares the 24 soil biome map with 0.25 degree resolution from the GEOS-Chem
259 settings to the new 12 km resolution soil biome map we created here for CMAQ. Table A2 gives
260 the biome type names with corresponding climate zones.

261 The classification of simulation domain into arid and non-arid region with consistent resolution
262 is also included in our implementation. Figure B1 shows the distribution of arid (red) and non-
263 arid (blue) regions. For the modeling grid classified as 'arid' region, the maximum moisture
264 scaling factor corresponds to the water-filled pore space (θ) value equal to 0.2; while for the
265 'non-arid' modeling grid, the maximum moisture scaling factor corresponds with θ=0.3
266 (Hudman et al., 2012).

267 ## 2.3 Representation of fertilizer N

268 We implemented two approaches for representing fertilizer N. The first approach regrids
269 fertilizer data from the global GEOS-Chem BDSNP implementation (Hudman et al. 2012) to our
270 12 km resolution CONUS domain. That scheme uses the global fertilizer database from Potter et
271 al. (2010) and assumed 37% of fertilizer and manure N is available (1.8 Tg-N yr^{-1}) for potential
272 emission. Figure B2 provides the day-by-day variation of total N remaining due to fertilizer
273 application over CONUS during a year, and shows the typical cycle between growing season and
274 non-growing season. The Potter data, however, are a decade old and at coarse resolution for
275 county-level in US.

276 Our second approach (Figure 3) uses the EPIC model as implemented in the FEST-C tool
277 (Cooter et al. 2012) to provide a dynamic representation of fertilizer applications for a specific
278 growing season. FEST-C (v1.1) generates model-ready fertilizer input files for CMAQ. . Use of

FEST-C/EPIC instead of soil emissions from YL scheme has been shown to improve CMAQ performance for nitrate and ammonia in CONUS (Bash et al., 2013). The BELD4 tool in FEST-C system was used to provide the crop usage fraction over our domain. We summed FEST-C data for ammonia, nitrate and organic, T1_ANH3, T1_ANO3 and T1_AON respectively in kg-N/ha, to give a total soil N pool for each of 42 simulated crops (CMAS, 2015). This daily crop-wise total soil N pool was then weighted by the fraction of each crop type at each modeling grid to get a final weighted sum total soil N pool usable in BDSNP. CMAQ v.5.0.2 can be run with in-line biogenic emissions, calculated in tandem with the rest of the model. Since the EPIC N pools already include N deposition, we designed our soil NO emissions module to be flexible in recognizing whether it is using fertilizer data such as Potter et al. (2010) that does not include deposition or EPIC that does.

Figure 4 compares the FEST-C derived N fertilizer map and the default coarser resolution long-term average fertilizer map from Potter. While the spatial patterns are similar, EPIC provides finer resolution and more up-to-date information.

2.4 Model configurations and data use for model evaluations

The CMAQ domain settings for CONUS as provided by the EPA were used to simulate the whole month of July in 2011. July corresponds to the month of peak flux for soil nitrogen emissions in the United States (Williams et al., 1992; Cooter et al., 2012; Bash et al., 2013) and is an active period for ozone photochemistry (Cooper et al., 2014; Strode et al., 2015).

A ten day (21 June-30 June, 2011) spin-up time was used to minimize the influence from initial conditions. The domain consisted of 396 columns, 246 rows, 26 vertical layers, and 12 km rectangular cells using a Lambert Conformal Projection over North America. This configuration was consistent throughout the WRF-BDSNP-CMAQ modeling framework (see Figure 1). Meteorology data were produced through the WRF Model nudged to National Centers for Environmental Prediction (NCEP) and National Center for Atmospheric Research Reanalysis (NARR) data, which is comprised of historical observations and processed to control quality and consistency across years by National Oceanic and Atmospheric Administration (NOAA).

Emissions were generated using the Sparse Matrix Operator Kernel Emissions (SMOKE) model (CMAS, 2014) and 2011NEIv1. CMAQ was applied with bi-directional exchange of ammonia between soils and atmosphere.

We applied CMAQ with three sets of soil NO emissions: a) Standard YL soil NO scheme, b) BDSNP scheme with Potter et al. (2010) fertilizer data set and biome mappings from GEOS-Chem, and c) BDSNP scheme with EPIC 2011 data and new biome mappings (see Appendix Table A3). Within these three cases, we simulated the impact of anthropogenic NO_x reductions applied to all contributing source sectors listed in the 2011 National Emission Inventory (NEI). For this purpose, we considered the baseline NO_x reduction scenario from 2011 to 2025 that EPA's Regulatory Impact Analysis (RIA) determined for Business as Usual (BAU) in the CONUS domain (Figure 2A-1, Table 2A-1 in https://www3.epa.gov/ttn/ecas/docs/20151001ria.pdf). Table 1 gives a full list of modeling configurations settings used for achieving the above-mentioned simulations.
Model simulations were evaluated against the following in situ and satellite-based data: 16 USEPA Clean Air Status and Trends Network (CASTNET) sites for MDA8 O_3 (www.epa.gov/castnet), 9 Interagency Monitoring of Protected Visual Environments (IMPROVE) sites for daily average $PM_{2.5}$ (Malm et al., 1994), and NASA's OMI retrieval product for tropospheric NO_2 column (Bucsela et al., 2013; Lamsal et al., 2014). Fig. 5 shows the spatial distribution of the ground sites used for validation of modeled estimates. The selected ground sites for model validation are mostly based in agricultural regions with intense fertilizer application rate and high NO fluxes, specifically the Midwest, southern plains, and San Joaquin Valley.

We also simulated three sensitivity cases for the same time period and domain with the offline soil NO module: a) NLCD40 based (new) biome vs GEOS-Chem based (old) biome (using EF1 in Table A1), b) EPIC 2011 vs Potter data and, c) Global mean biome emission factor (EF1 in Table A1) vs North American mean emission factor (EF3 in Table A1) (Supplementary material Section S.3).

3 Results and Discussion

3.1 Spatial distribution of nitrogen fertilizer application and soil NO emissions over CONUS

We demarcated the CONUS domain into six sub-domains (Figure 6) to analyze model outputs. The updated BDSNP model and EPIC fertilizer result in higher soil NO emission rates than YL and Potter. Emissions increase by a factor ranging from 1.8 to 2.8 in shifting from YL to BDSNP, even while retaining the Potter fertilizer data and original biome map, indicating that the shift from YL to BDSNP scheme is the largest driver of the increase in emissions estimates. EPIC and the new biome dataset further increase emissions over most of CONUS, except for the southwest region. In Midwest and Western US, the new biome map identified more cropland and shifted some grasslands to other land cover types such as forests, savannah and croplands, which exhibit higher soil NO emissions (Figure 2; Table A1). The Midwest region is characterized with the highest emission rate due to its abundant agricultural lands with high fertilizer application rates (Figure 4).

3.2 Evaluation of CMAQ NO_2 with satellite OMI NO_2 observations

The standard (version 2.1) OMI tropospheric NO_2 column observations from NASA's Aura satellite as discussed in Bucsela et al. (2013) and Lamsal et al. (2014) were used for comparison with our modelled NO_2 vertical columns. To enable comparison, the quality-assured, clear-sky (cloud radiance fraction < 0.5) OMI NO_2 data were gridded and projected to our domain by using ArcGIS 10.3. CMAQ modelled NO_2 column densities in molecules per cm^2 were derived using vertical integration and extracted for 13:00-14:00 local time, corresponding to the time of OMI measurements.

We compared CMAQ simulated tropospheric NO_2 columns with OMI product for regions showing highest sensitivity in soil NO switching from YL to BDSNP: Midwest, San Joaquin Valley in California and central Texas (see Appendix Figure B3). Switching from YL to our updated BDSNP ('new') module improved agreement with OMI NO_2 columns in central Texas but over-predicts column NO_2 in the San Joaquin Valley and Midwest (Figure 7). Even the YL

estimate was higher than OMI by a factor of two in the Midwest (Figure 7). Vinken et al. (2014) found the Midwest U.S. to be one of the few regions globally where a BDSNP-based inventory over-predicted soil NO emissions inferred from OMI.

3.3 Evaluation with $PM_{2.5}$ and ozone observations

Model results are compared with observational data from IMPROVE monitors for $PM_{2.5}$ and CASTNET monitors for ozone. We first compute differences between ozone and $PM_{2.5}$ estimates from the three simulation cases to identify sites influenced by the choice of soil NO scheme during our July 2011 episode (Figures 8 and 9). Overall, analysis of variance and a t-test showed no statistically significant differences among the soil NO cases for $PM_{2.5}$, but found the YL case to be significantly different ($p<<0.05$) from the BDSNP cases for ozone. Closer examination highlights nine IMPROVE sites for $PM_{2.5}$ and 16 CASTNET sites for ozone (Figures 5, 8 and 9) where CMAQ results are sensitive to soil NO changes (Figure 6).

Statistical comparisons of modeled and observed daily average $PM_{2.5}$ at the nine IMPROVE sites are provided in Table 2. Mean Absolute Gross Error (MAGE) and Root Mean Square Error (RMSE) improved from 2.8 to 2.7 ug/m^3 and 3.4 to 3.3 ug/m^3 respectively when moving from YL to BDSNP with the new inputs. Both Pearson's and Spearman's ranked correlation coefficient (R) shows no significant change when soil NO module in CMAQ is switched from YL to BDSNP (Potter with old biome) and BDSNP (EPIC with new biome) (Tables 2). Use of the ranked correlation coefficient minimizes the impact of spurious correlations due to outliers but does not affect the analysis. Switching from YL to our updated BDSNP ('new') module shows that the predicted versus observed fit becomes slightly closer to 1:1 (Figure 10). Numerical Mean Bias (NMB) and Numerical Mean Error (NME) improve from -28.5% to -26.4% and 34.6% to 33.6%, respectively.

In contrast to the $PM_{2.5}$ results, the updated soil NO scheme yields mixed impacts on model performance for maximum daily average 8-hour (MDA8) ozone at the targeted 16 CASTNET sites (Table 3 and Figure 11). For the 11 agricultural/prairie sites, replacement of YL with BDSNP with new inputs increases NMB from 7.6% to 14.1% and NME from 15.7 to 19.3% (Table 3). The excess ozone may occur because FEST-C does not account for the loss of

fertilizer N to the water stream ("tile drainage") in wet conditions (Dinnes et al., 2002). Hudman et al. (2012) suggested $\theta = 0.175$ (m^3/m^3) as threshold below which dry condition occur. During July 2011, in Midwest monthly mean soil moisture (θ_{mean}, m^3/m^3) is mostly > 0.175, indicating possibility of wet conditions (Fig. S5). Overestimation of O_3 is due to higher NO emissions, as these regions comprise of mostly NO_x limited rural locations.

At the California CASTNET sites, BDSNP enhances model performance in simulating observed MDA8 ozone (Table 3). This can be seen in the NMB, NME, MAGE, and RMSE comparisons between YL and BDSNP, though updating BDSNP to the newer inputs does not enhance performance (Table 3).

3.4 Impact of soil NO scheme on ozone sensitivity to anthropogenic NO_x perturbations

We analyzed how the choice of soil NO parameterization affects the responsiveness of ozone to reductions in anthropogenic NO_x emissions. We applied emission perturbation factors based on the 5.7 million ton reduction in baseline anthropogenic NO_x emissions from 2011 to 2025 that US EPA simulated in its latest RIA (U.S. EPA, 2015). Table 4 gives the perturbation factors we used to obtain baseline anthropogenic NO_x emissions for 2025 over all contributing sectors as listed from NEI 2011. Since our simulation is for July 2011 over CONUS, we used these perturbation factors rather than the net reductions in RIA to scale emissions in a similar pattern as given in RIA for annual baseline perturbations from 2011 to 2025 with BAU.

Shifting from YL to the BDSNP soil NO scheme reduces the sensitivity of MDA8 O_3 to anthropogenic NO_x perturbations. The impacts are greatest in California and the Midwest, where shifting to BDSNP can reduce the expected impact of the anthropogenic NO_x reductions by ~ 1 to 1.5 ppbV. Changing the inputs within the BDSNP scheme has a smaller impact (Figure 12). Our results imply that the higher soil NO emissions from our updated BDSNP module shifts the ozone photochemistry to a less strongly NO_x-limited regime.

4 Conclusions

Our BDSNP implementation represents a substantial update from the YL scheme for estimating soil NO in CMAQ. Compared to the previous implementation of BDSNP in global GEOS-Chem model, our implementation in CMAQ incorporated finer-scale representation of its dependence on land use, soil conditions, and N availability. This finer resolution and updated biome and fertilizer data set resulted in higher sensitivity of soil NO to biome emission factors. Our updated BDSNP scheme (EPIC and new biome) predicts slightly higher soil NO than the inputs used in GEOS-Chem, primarily due to the use of 2011 daily EPIC/FEST-C fertilizer data and fine resolution NLCD40 biomes (Figure 6).

Sensitivities to different input datasets were examined using our offline BDSNP module to reduce computational cost. Switching from GEOS-Chem biome to new NLCD40 biome drops soil NO in the northwest and southwest portions of our domain due to the finer resolution biome map exhibiting lower emission factors in those regions. Replacing fertilizer data from Potter et al. (2010) with an EPIC 2011 dataset increased soil NO mostly in the Midwest (Supplementary material Figure S4).

We compared CMAQ tropospheric NO_2 column densities to OMI observations as spatial averages, focusing on regions sensitive to the switch from YL to our updated BDSNP scheme. Temporal average of OMI and CMAQ simulated NO_2 column densities was done over the OMI overpass time (13:00-14:00 local time) for July 2011 monthly mean. Figure 7 summarizes tropospheric NO_2 column density comparisons between model and OMI satellite observation for aforementioned sensitive regions. Central Texas showed improvement with switch from YL to our BDSNP ('new') scheme. For July 2011, central Texas and San Joaquin Valley exhibit relatively dry soil conditions, whereas the Midwest was mostly wet (Supplementary material Figure S5). Even with similar conditions as central Texas, San Joaquin region shows overall degradation. Overestimation of simulated NO_2 columns up to twice of OMI over Midwestern US and San Joaquin valley for summer episodes has been exhibited earlier as well (Lamsal et al., 2014). Several factors, such as spatial inhomogeneity within OMI pixels and possible errors arising from the stratosphere-troposphere separation scheme and air mass factor calculations, can be attributed to this overestimation. Retrieval difficulties in complex terrain may explain the

discrepancies in NO_2 column over San Joaquin Valley even though it shows slight improvement with updates within BDSNP ('old' to 'new') and has similar dry conditions as central Texas.

We examined the performance of CMAQ under each of the soil NO parameterizations. Regions where soil NO parameterizations most impacted MDA8 ozone and $PM_{2.5}$ were examined for model performance in simulating CASTNET MDA8 O_3 and IMPROVE $PM_{2.5}$ observations.

For $PM_{2.5}$, our updated BDSNP module ('new') showed the best performance (Table 2). Evaluations against MDA8 O_3 observations found contrasting behavior for two different sets of CASTNET sites. The 11 mostly agricultural and prairie sites extending across the Midwest and southern US showed consistent overestimation as we moved from YL to BDNSP with new inputs, with bias jumping from ~ 7% to 14% and error from 15% to 19% (Table 3). However, the 5 forest/national park sites most of which lie near the San Joaquin Valley by contrast showed an overall improvement in bias from ~ 13% to 10% and in error from ~ 17 % to 15% (Table 3).

Over-predictions of soil NO emissions especially in wet conditions may result from EPIC not properly accounting for on-farm nitrogen management practices like tile drainage. Crops such as alfalfa, hay, grass, and rice experience soil N loss due to tile drainage in wet soils (Gast et al., 1978; Randall et al., 1997). Recent updates to FEST-C (v. 1.2) include tile drainage for some crops but not hay, rice, grass and alfalfa (CMAS, 2015). Tile drainage results in loss of fertilizer N to water run-off from wet or moist soils.

We analyzed how the soil NO schemes affect the sensitivity of MDA8 ozone to anthropogenic NO_x reductions by considering the 5.7 million tons/year reduction from 2011 levels that U.S. EPA expects for United States by 2025 with BAU scenario. These reductions were applied on basis of perturbation factors of relevant sectors keeping biogenic emissions unchanged for July 2011, based on EPA's annual baseline estimates between 2011 and 2025 (Table 4). These anthropogenic NO_x reductions yield less reduction in MDA8 O_3 under the BDNSP soil NO scheme than YL, with 1-2 ppbv differences over parts of California and the Midwest (Figure 12). The shift occurs because our updated BDSNP schemes have higher soil NO in these regions, pushing them toward less strongly NO_x-limited regimes.

This work represents crucial advancement toward enhanced representation of soil NO in a regional model. Although possible wet biases and using dominant land cover rather than fractional in soil biome classification, may have over-predicted NO in agricultural regions in present study. The EPIC simulation used here lacks complete representation of farming management practices like tile, which can reduced soil moisture and soil NO fluxes. Inclusion of biogeochemistry influencing different reactive N species encompassing the entire N cycling could enable more mechanistic representation of emissions. For future work, there is a need for more accurate representation of actual farming practices and internalizing updated soil reactive N bio-geochemical schemes. More field observations are needed as well in order to increase the sample size for evaluation of modeled estimates soil emissions of reactive N species beyond NO.

Code availability

The modified and new scripts used for implementation of BDSNP in CMAQ Version 5.0.2 are in the supplementary material. Also provided as supplement is the user manual giving details on implementing BDSNP module in-line with CMAQ, as used in this work. Source codes for CMAQ version 5.0.2 and FEST-C version 1.1 are both open-source, available with applicable free registration at http://www.cmascenter.org. Advanced Research WRF model (ARW) version 3.6.1 used in this study is also available as a free open-source resource at http://www2.mmm.ucar.edu/wrf/users/download/get_source.html.

Acknowledgements

This work was supported by NASA's Air Quality Applied Sciences Team through a tiger team project grant for DYNAMO: DYnamic Inputs of Natural Conditions for Air Quality Models and by the Texas Air Quality Research Program. Although this work was reviewed by EPA and approved for publication, it may not necessarily reflect official Agency policy.

References

Bash, J., Cooter, E., Dennis, R., Walker, J., and Pleim, J.: Evaluation of a regional air-quality model with bidirectional NH 3 exchange coupled to an agroecosystem model, Biogeosciences, 10, 1635-1645, 2013.

Bey, I., Jacob, D. J., Yantosca, R. M., Logan, J. A., Field, B., Fiore, A. M., Li, Q., Liu, H., Mickley, L. J., and Schultz, M.: Global modeling of tropospheric chemistry with assimilated meteorology: Model description and evaluation, J. Geophys. Res., 106, 23,073-23,096, 2001.

Boersma, K., Jacob, D. J., Bucsela, E., Perring, A., Dirksen, R., Yantosca, R., Park, R., Wenig, M., Bertram, T., and Cohen, R.: Validation of OMI tropospheric NO 2 observations during INTEX-B and application to constrain NO_x emissions over the eastern United States and Mexico, Atmospheric Environment, 42, 4480-4497, 2008.

Bucsela, E. J., Krotkov, N. A., Celarier, E. A., Lamsal, L. N., Swartz, W. H., Bhartia, P. K., Boersma, K. F., Veefkind, J. P., Gleason, J. F., and Pickering, K. E.: A new stratospheric and tropospheric NO2 retrieval algorithm for nadir-viewing satellite instruments: applications to OMI, Atmos. Meas. Tech., 6, 2607-2626, doi:10.5194/amt-6-2607-2013, 2013.

Byun, D. W. and Schere, K. L.: Review of the governing equations, computational algorithms, and other components of the models- 3 Community Multiscale Air Quality (CMAQ) modeling system, Appl. Mech. Rev., 59, 51–77, 2006.

Conrad R. Soil microorganisms as controllers of atmospheric trace gases (H_2, CO, CH_4, OCS, N_2O, and NO). *Microbiological Reviews*. 60(4):609-640; 1996.

Cooper, O.R., Parrish, D.D., Ziemke, J., Balashov, N.V., Cupeiro, M., Galbally, I.E., Gilge, S., Horowitz, L., Jensen, N.R., Lamarque, J.F. and Naik, V.: Global distribution and trends of tropospheric ozone: An observation-based review. Elementa: Science of the Anthropocene, 2(1), p.000029, 2014.

Cheng, J.-l., Zhou, S., and Zhu, Y.-w.: Assessment and mapping of environmental quality in agricultural soils of Zhejiang Province, China, Journal of Environmental Sciences, 19, 50-54, 2007.

CMAS, Sparse Matrix Operators Kernel Emissions model (SMOKE) version 3.6, University of North Carolina at Chapel Hill Institute for the Environment, Center for Environmental Modeling for Policy Development (CEMPD), Community Modeling and Analysis System Center (CMAS), Chapel Hill, NC (http://www.smoke-model.org), 2014.

528 CMAS 2015: User's Guide for the Fertilizer Emission Scenario Tool for CMAQ (FEST-C) Version 1.2,
529 Institute of Environment, The University of North Carolina at Chapel Hill, Chapel Hill, NC, available at:
530 https://www.cmascenter.org/fest-c/documentation/1.2/FESTC1_2_userManual.pdf, last accessed: 30
531 September, 2015

532 Cooter, E. J., Bash, J.O., Benson, V., and Ran, L.: Linking agricultural crop management and air quality
533 models for regional to national-scale nitrogen assessments. *Biogeosciences*, 9, no. 10: 4023-4035, 2012.

534 Davidson, E.: Pulses of nitric oxide and nitrous oxide flux following wetting of dry soil: an assessment of
535 probable sources and importance relative to annual fluxes, Ecol. Bull., 42, 149–155, 1992.

536 Davidson, E. and Kingerlee, W.: A global inventory of nitric oxide emissions from soils, Nutr. Cycl.
537 Agroecosys., 48, 37–50, doi:10.1023/A:1009738715891, 1997.

538 Delon, C., Serça, D., Boissard, C., Dupont, R., Dutot, A., Laville, P., De Rosnay, P., and Delmas, R.: Soil NO
539 emissions modelling using artificial neural network, Tellus B, 59, 502-513, 2007.

540 Delon, C., Reeves, C., Stewart, D., Serça, D., Dupont, R., Mari, C., Chaboureau, J.-P., and Tulet, P.:
541 Biogenic nitrogen oxide emissions from soils–impact on NO x and ozone over West Africa during AMMA
542 (African Monsoon Multidisciplinary Experiment): modelling study, Atmospheric Chemistry and Physics,
543 8, 2351-2363, 2008.

544 Dinnes, D. L., Karlen, D. L., Jaynes, D. B., Kaspar, T. C., Hatfield, J. L., Colvin, T. S., and Cambardella, C. A.:
545 Nitrogen management strategies to reduce nitrate leaching in tile-drained Midwestern soils, Agronomy
546 journal, 94, 153-171, 2002.

547 Galloway, J. N., and Cowling, E. B.: Reactive nitrogen and the world: 200 years of change, AMBIO: A
548 Journal of the Human Environment, 31, 64-71, 2002.

549 Gast, R., Nelson, W., and Randall, G.: Nitrate accumulation in soils and loss in tile drainage following
550 nitrogen applications to continuous corn, Journal of environmental quality, 7, 258-261, 1978.

551 Harrison, R. M., Yamulki, S., Goulding, K., and Webster, C.: Effect of fertilizer application on NO and N2O
552 fluxes from agricultural fields, Journal of Geophysical Research: Atmospheres (1984–2012), 100, 25923-
553 25931, 1995.

554 Hudman, R. C., Moore, N. E., Mebust, A. K., Martin, R. V., Russell, A. R., Valin, L. C., and Cohen, R. C.:
555 Steps towards a mechanistic model of global soil nitric oxide emissions: implementation and space

based-constraints, Atmos. Chem. Phys., 12, 7779– 7795, doi:10.5194/acp-12-7779-2012, 2012. Hudman, R. C., Russell, A. R., Valin, L. C., and Cohen, R. C.: Interannual variability in soil nitric oxide emissions over the United States as viewed from space, Atmos. Chem. Phys., 10, 9943– 9952, doi:10.5194/acp-10-9943-2010, 2010.

IFIA: International Fertilizer Industry Association 2001. Nitrogen, phosphate and potash statistics.(http://www.fertilizer.org/ifa/statistics/IFADATA/dataline.asp), 2001.

IPCC: Climate Change 2007: Impacts, Adaptation and Vulnerability, Contribution of Working Group II to the Fourth Assessment Report of the Intergovernmental Panel on Climate Change, edited by: Parry, M. L., Canziani, O. F., Palutikof, J. P., van der Linden, P. J., and Hanson, C. E., Cambridge University Press, Cambridge, UK, 976 pp., 2007.

Jaeglé, L., Martin, R. V., Chance, K., Steinberger, L., Kurosu, T. P., Jacob, D. J., Modi, A. I., Yoboué, V., Sigha-Nkamdjou, L., and Galy-Lacaux, C.: Satellite mapping of rain-induced nitric oxide emissions from soils, J. Geophys. Res.-Atmos., 109, D21310, doi:10.1029/2004JD004787, 2004.

Jaeglé, L., Steinberger, L., Martin, R. V., and Chance, K.: Global partitioning of NO x sources using satellite observations: Relative roles of fossil fuel combustion, biomass burning and soil emissions, Faraday Discussions, 130, 407-423, 2005.

Kesik, M., Blagodatsky, S., Papen, H., and Butterbach-Bahl, K.: Effect of pH, temperature and substrate on N2O, NO and CO2 production by Alcaligenes faecalis p, Journal of applied microbiology, 101, 655-667, 2006.

Kottek, M., Grieser, J., Beck, C., Rudolf, B., and Rubel, F.: World Map of the Köppen-Geiger climate classification updated. *Meteorologische Zeitshrift*, 15, 259-263. DOI: 10.1127/0941-2948/2006/0130, 2006.

Lamsal, L., Krotkov, N., Celarier, E., Swartz, W., Pickering, K., Bucsela, E., Gleason, J., Martin, R., Philip, S., and Irie, H.: Evaluation of OMI operational standard NO 2 column retrievals using in situ and surface-based NO 2 observations, Atmospheric Chemistry and Physics, 14, 11587-11609, 2014.

Li, Y., Schichtel, B.A., Walker, J.T., Schwede, D.B., Chen, X., Lehmann, C.M., Puchalski, M.A., Gay, D.A. and Collett, J.L.: Increasing importance of deposition of reduced nitrogen in the United States. Proceedings of the National Academy of Sciences, 5874-5879, doi: 10.1073/pnas.1525736113, 2016.

584 Lin, J.-T.: Satellite constraint for emissions of nitrogen oxides from anthropogenic, lightning and soil
585 sources over East China on a high-resolution grid, Atmospheric Chemistry and Physics, 12, 2881-2898,
586 2012.

587 Ludwig, J., Meixner, F., Vogel, B., and Förstner, J.: Soil-air exchange of nitric oxide: an overview of
588 processes, environmental factors, and modeling studies, Biogeochemistry, 52, 225–257,
589 doi:10.1023/A:1006424330555, 2001.

590 Miyazaki, K., Eskes, H. J., and Sudo, K.: Global NO_x emission estimates derived from an assimilation of
591 OMI tropospheric NO2 columns, Atmos. Chem. Phys., 12, 2263–2288, doi:10.5194/acp- 12-2263-2012,
592 2012.

593 Malm, W. C., Sisler, J. F., Huffman, D., Eldred, R. A., and Cahill, T. A.: Spatial and seasonal trends in
594 particle concentration and optical extinction in the United States, JOURNAL OF GEOPHYSICAL
595 RESEARCH-ALL SERIES-, 99, 1347-1347, 1994.

596 Otte, T. L. and Pleim, J. E.: The Meteorology-Chemistry Interface Processor (MCIP) for the CMAQ
597 modeling system: updates through MCIPv3.4.1, Geosci. Model Dev., 3, 243-256, doi:10.5194/gmd-3-
598 243-2010, 2010.

599 Parton, W. J., Holland, E. A., Del Grosso, S. J., Hartman, M. D., Martin, R. E., Mosier, A. R., Ojima, D. S.,
600 and Schimel, D. S.: Generalized model for NO_x and N_2O emissions from soils, J. Geophys. Res.-Atmos.,
601 106, 17403–17419, doi:10.1029/2001JD900101, 2001.

602 Pilegaard, K.: Processes regulating nitric oxide emissions from soils, Philosophical Transactions of the
603 Royal Society B: Biological Sciences, 368, 20130126, 2013.

604 Pleim, J.E. and Xiu, A.: Development of a land surface model. Part II: Data assimilation. Journal of
605 Applied Meteorology, 42(12), pp.1811-1822, 2003.

606 Potter, C., Matson, P., Vitousek, P., and Davidson, E.: Process modeling of controls on nitrogen trace gas
607 emissions from soils worldwide, J. Geophys. Res.-Atmos., 101, 1361–1377, doi:10.1029/95JD02028,
608 1996.

609 Potter, P., Navin, R., Elena M. B., and Simon D. D.: Characterizing the spatial patterns of global fertilizer
610 application and manure production. *Earth Interactions*, 14, no. 2: 1-22, 2010.

611 Randall, G., Huggins, D., Russelle, M., Fuchs, D., Nelson, W., and Anderson, J.: Nitrate losses through
612 subsurface tile drainage in conservation reserve program, alfalfa, and row crop systems, Journal of
613 Environmental Quality, 26, 1240-1247, 1997.

614 Scholes, M., Martin, R., Scholes, R., Parsons, D., and Winstead, E.: NO and N_2O emissions from savanna
615 soils following the first simulated rains of the season, Nutr. Cycl. Agroecosys., 48, 115– 122,
616 doi:10.1023/A:1009781420199, 1997.

617 Seinfeld, John H., and Spyros N. Pandis. Atmospheric chemistry and physics: from air pollution to climate
618 change. John Wiley & Sons, 2012.

619 Shepherd, M., Barzetti, S., and Hastie, D.: The production of atmospheric NO x and N 2 O from a
620 fertilized agricultural soil, Atmospheric Environment. Part A. General Topics, 25, 1961-1969, 1991.

621 Skamarock, W. C., Klemp, J. B., Dudhia, J., Gill, D. O., Barker, D. M., Duda, M. G., Huang, X., Wang, W.,
622 and Powers, J. G.: A description of the advanced research WRF version 3, NCAR Tech. Note, NCAR/TN-
623 475+STR, 8 pp., Natl. Cent. for Atmos. Res., Boulder, Colo., 2008 (available at:
624 http://www.mmm.ucar.edu/wrf/users/docs/arw_v3.pdf)

625 Stehfest, E., & Bouwman, L.: N_2O and NO emission from agricultural fields and soils under natural
626 vegetation: summarizing available measurement data and modeling of global annual emissions. Nutrient
627 Cycling in Agroecosystems, 74(3), 207-228.doi: 10.1007/s10705-006-9000-7, 2006.

628 Steinkamp, J., & Lawrence, M. G.: Improvement and evaluation of simulated global biogenic soil NO
629 emissions in an AC-GCM. Atmospheric Chemistry and Physics, 11(12), 6063–6082. doi:10.5194/acp-11-
630 6063-2011, 2011.

631 Stavrakou, T., Müller, J.-F., Boersma, K. F., De Smedt, I., and van der A, R. J.: Assessing the distribution
632 and growth rates of NO_x emission sources by inverting a 10 year record of NO2 satellite columns,
633 Geophys. Res. Lett., 35, L10801, doi:10.1029/2008GL033521, 2008.

634 Stavrakou, T., Müller, J.F., Boersma, K. F., van der A, R. J., Kurokawa, J., Ohara, T., and Zhang, Q.: Key
635 chemical NO_x sink uncertainties and how they influence top-down emissions of nitrogen oxides, Atmos.
636 Chem. Phys., 13, 9057–9082, doi:10.5194/acp-13-9057-2013, 2013.

637 Strode, S. A., Rodriguez, J. M., Logan, J. A., Cooper, O. R., Witte, J. C., Lamsal, L. N., Damon, M., Van
638 Aartsen, B., Steenrod, S. D., and Strahan, S. E.: Trends and variability in surface ozone over the United
639 States, J. Geophys. Res. Atmos., 120, 9020–9042, doi:10.1002/2014JD022784, 2015.

640 Su, H., Cheng, Y., Oswald, R., Behrendt, T., Trebs, I., Meixner, F. X., Andreae, M. O., Cheng, P., Zhang, Y.,
641 and Pöschl, U.: Soil nitrite as a source of atmospheric HONO and OH radicals, Science, 333, 1616-1618,
642 2011.

643 USDA ERS: USDA ERS (United States Department of Agriculture, Economic Research Service) Data sets:
644 U.S. fertilizer use and price. Last updated July 12, 2013. http://www.ers.usda.gov/data-
645 products/fertilizer-use-and-price.aspx, 2013.

646 U.S. Environmental Protection Agency, Clean Air Markets Division, Clean Air Status and Trends Network
647 (CASTNET)[Ozone 8-Hour Daily Max] available at www.epa.gov/castnet. Date accessed: [July, 2011]

648 U.S. EPA : U.S. Environmental Protection Agency, 2015. Regulatory Impact Analysis of the Final
649 Revisions to the National Ambient Air Quality Standards for Ground-Level Ozone. EPA-452/R-15-007.
650 Office of Air Quality Planning and Standards, Research Triangle Park, NC. Last updated: March, 2016.
651 Available at: https://www3.epa.gov/ttn/ecas/docs/20151001ria.pdf .

652 van Dijk, S. M., A. Gut, G. A. Kirkman, B. M. Gomes, F. X. Meixner, and M. O. Andreae, Biogenic NO
653 emissions from forest and pasture soils: Relating laboratory studies to field measurements, J. Geophys.
654 Res., 107(D20), 8058, doi:10.1029/2001JD000358, 2002.

655 Veldkamp, E., and Keller, M.: Fertilizer-induced nitric oxide emissions from agricultural soils, Nutrient
656 Cycling in Agroecosystems, 48, 69-77, 1997.

657 Vinken, G. C. M., Boersma, K. F., Maasakkers, J. D., Adon, M., & Martin, R. V. (2014). Worldwide biogenic
658 soil NO_x emissions inferred from OMI NO_2 observations. Atmospheric Chemistry and Physics, 14(18),
659 10363–10381. doi:10.5194/acp-14-10363-2014.

660 Wang, Y., Logan, J. A., and Jacob, D. J.: Global simulation of tropospheric O3-NO x-hydrocarbon
661 chemistry: 2. Model evaluation and global ozone budget, Journal of Geophysical Research: Atmospheres
662 (1984–2012), 103, 10727-10755, 1998.

663 Wang, Y., McElroy, M. B., Martin, R. V., Streets, D. G., Zhang, Q., and Fu, T. M.: Seasonal variability of
664 NO_x emissions over east China constrained by satellite observations: Implications for combustion and
665 microbial sources, Journal of Geophysical Research: Atmospheres (1984–2012), 112, 2007.

666 Wang, Y., Zhang, Q. Q., He, K., Zhang, Q., and Chai, L.: Sulfate-nitrate-ammonium aerosols over China:
667 response to 2000–2015 emission changes of sulfur dioxide, nitrogen oxides, and ammonia, Atmos.
668 Chem. Phys., 13, 2635-2652, doi:10.5194/acp-13-2635-2013, 2013.

669 Williams, E. J., Parrish, D. D., Buhr, M. P., Fehsenfeld, F. C., and Fall, R.: Measurement of soil NO_x
670 emissions in central Pennsylvania, J. Geophys. Res.-Atmos., 93, 9539–9546,
671 doi:10.1029/JD093iD08p09539, 1988.

672 Williams, E. J., A. Guenther, F. C. Fehsenfeld, An inventory of nitric oxide emissions from soils in the
673 United States, J. Geophys. Res., 97, 7511–7519, 1992.

674 Yienger, J., and Levy, H.: Empirical model of global soil-biogenic NO~ x emissions, JOURNAL OF
675 GEOPHYSICAL RESEARCH-ALL SERIES-, 100, 11,447-411,447, 1995.

676 Zhang, W., Mo, J., Yu, G., Fang, Y., Li, D., Lu, X., and Wang, H.: Emissions of nitrous oxide from three
677 tropical forests in Southern China in response to simulated nitrogen deposition, Plant and Soil, 306, 221-
678 236, 2008.

679 .

680

681 Zhao, C., and Wang, Y.: Assimilated inversion of NO_x emissions over East Asia using OMI NO_2 column
682 measurements, Geophysical Research Letters, 36, 2009.

683

684 Zörner, J., Penning de Vries, M., Beirle, S., Sihler, H., Veres, P. R., Williams, J., and Wagner, T.: Multi-
685 satellite sensor study on precipitation-induced emission pulses of NO_x from soils in semi-arid
686 ecosystems, Atmos. Chem. Phys., 16, 9457-9487, doi:10.5194/acp-16-9457-2016, 2016.

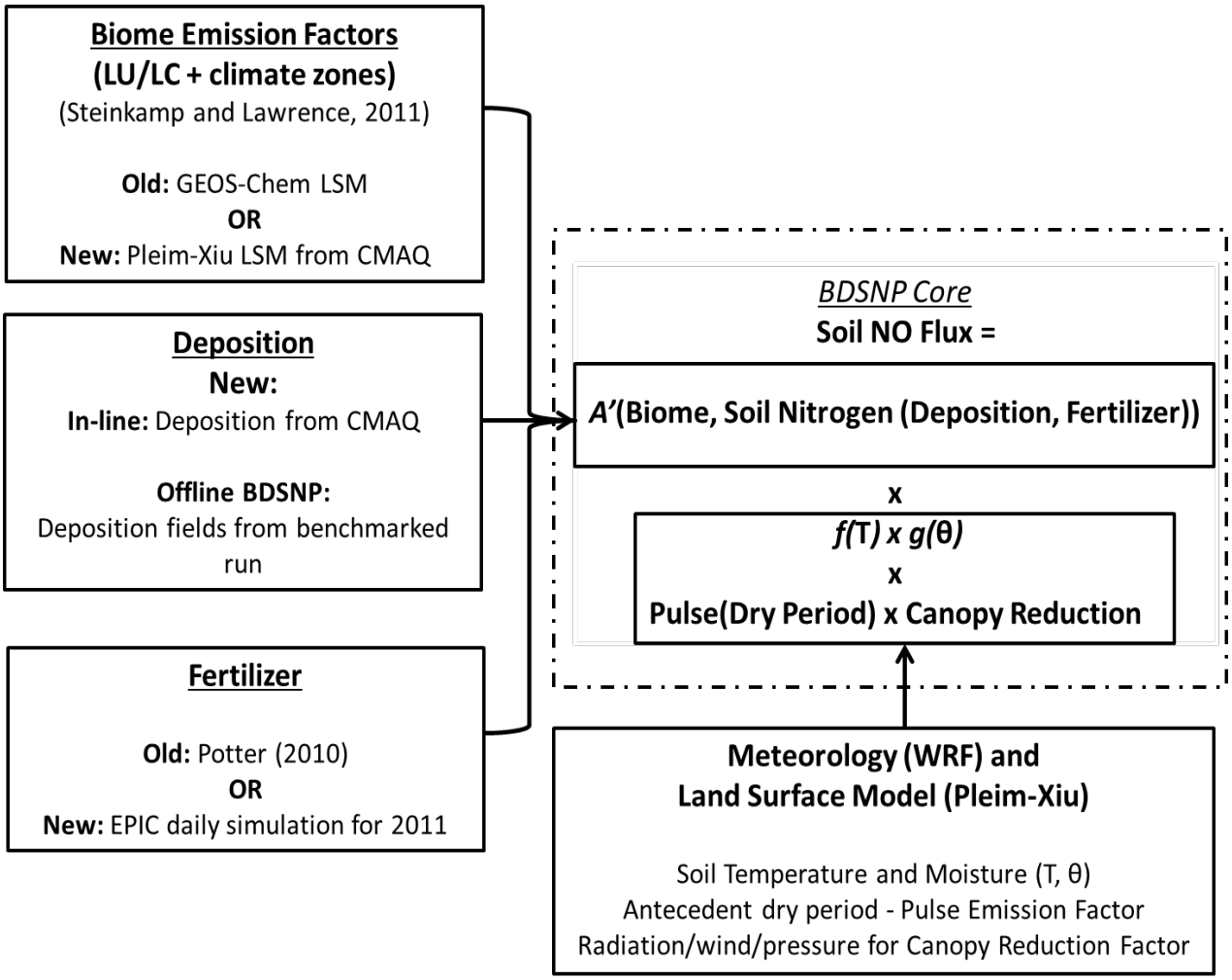

687

688

689 **Figure 1** Soil NO emissions modeling framework as implemented offline or in CMAQ (inline).
690 "Old" refers to the Hudman et al. (2012) implementation in GEOS-Chem. "New" refers to our
691 implementation in CMAQ.

692

693

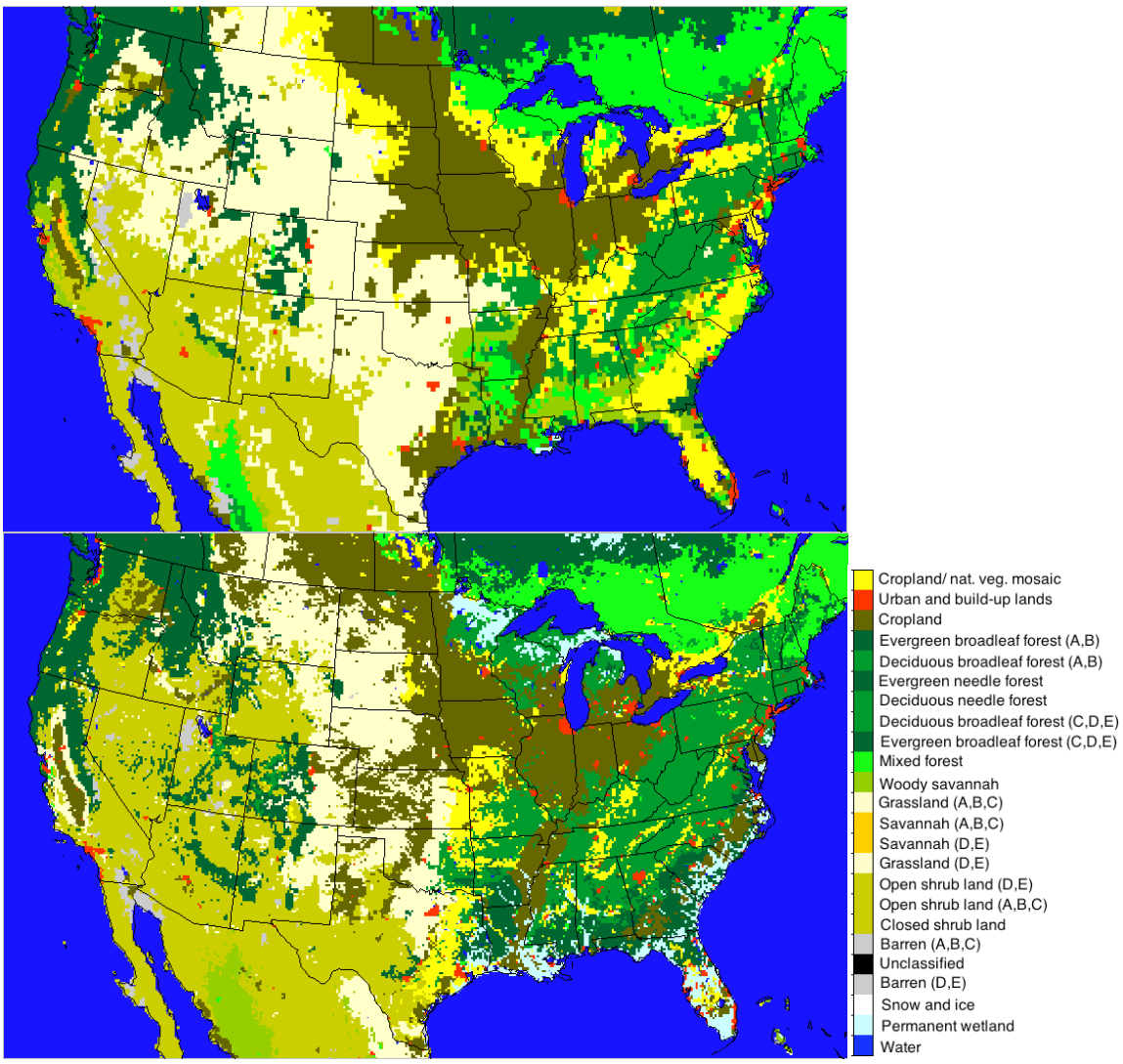

Figure 2 Biomes from GEOS-Chem (0.25° x 0.25°; top) and CMAQ MODIS NLCD40 (12 km x 12 km; bottom) regrouped to match the classifications for which emission factors are available from Steinkamp and Lawrence (2011). See Tables A1 and A2 (right) for the mappings between classifications. The color-bar legends for classifications are as per NLCD definitions (http://www.mrlc.gov/nlcd11_leg.php).

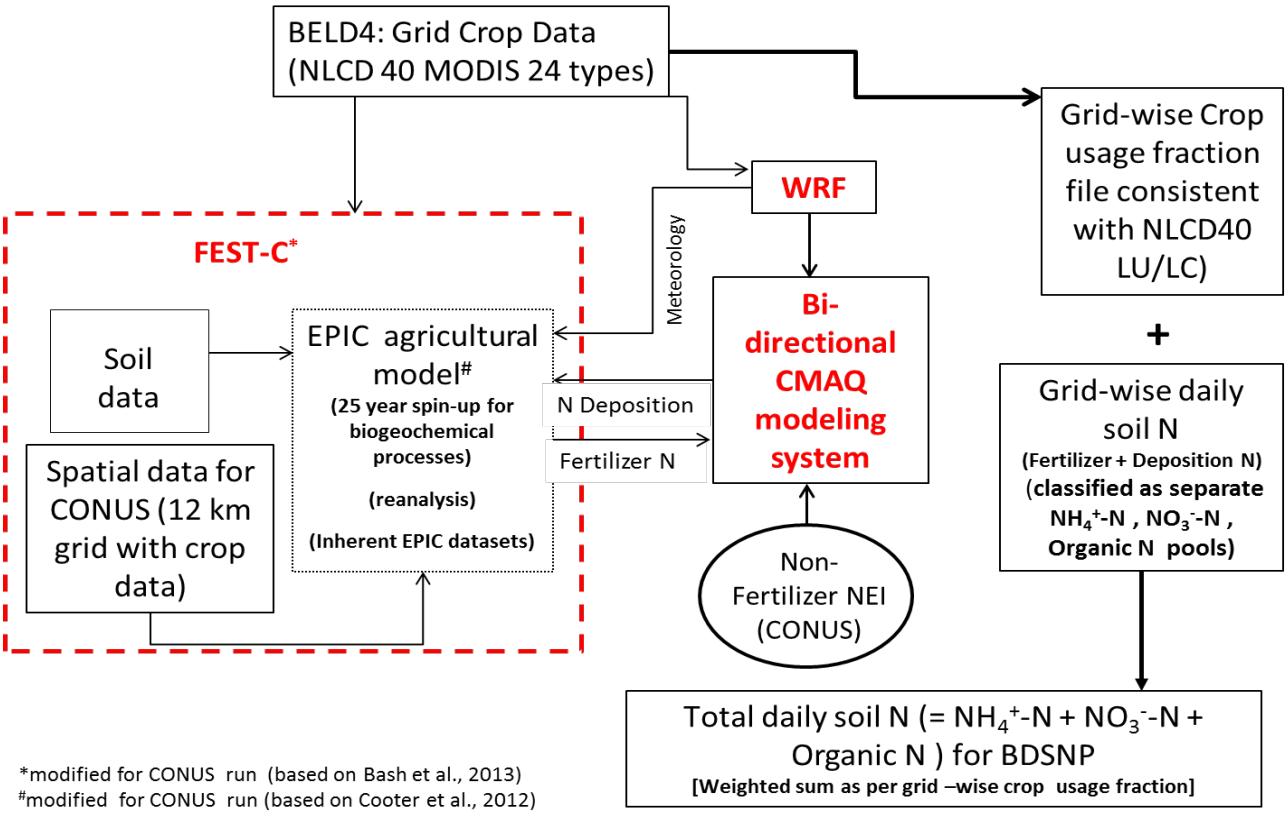

704

705 **Figure 3** Modeling framework for obtaining total soil N from EPIC using FEST-C.

706

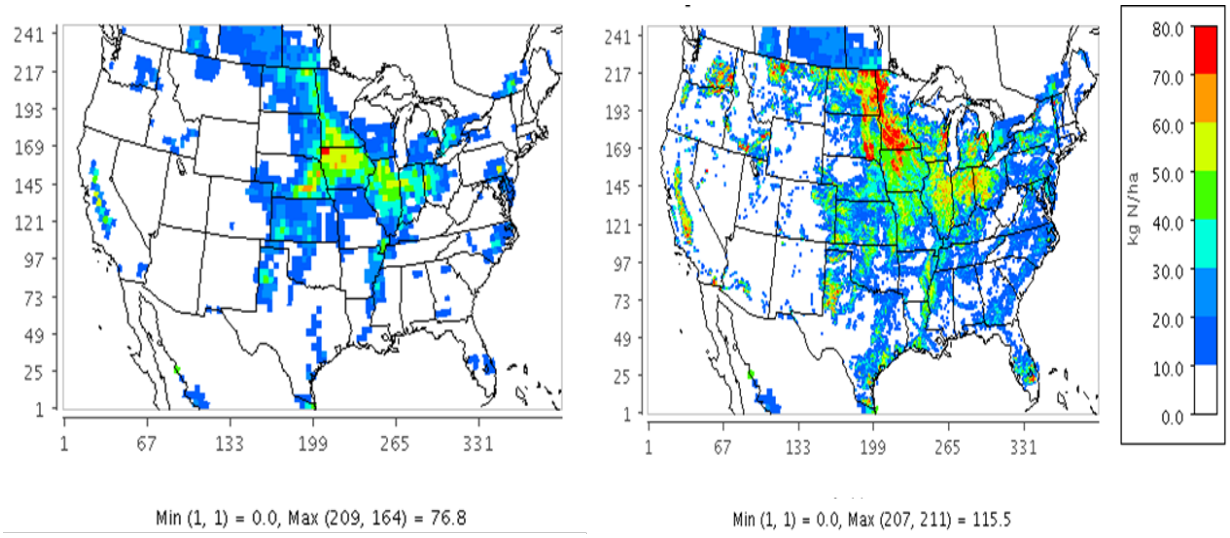

Figure 4 Potter (left) and EPIC (right) annual fertilizer application (Kg N/ha). Since EPIC modeled only the U.S., Potter et al. (2010) is used in both cases to represent Canada and Mexico.

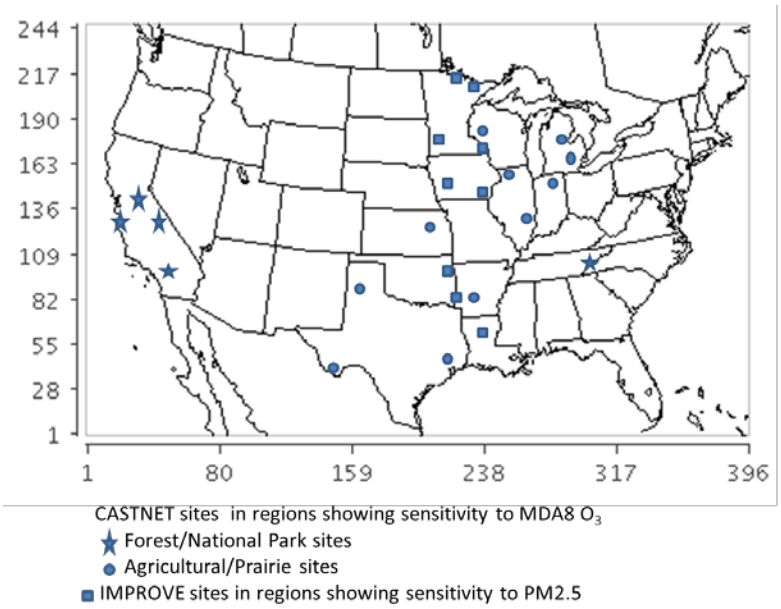

Figure 5 CASTNET (Forest/National Park and agricultural sites) and IMPROVE sites in continental US for comparison of modeled and observed ozone and $PM_{2.5}$.

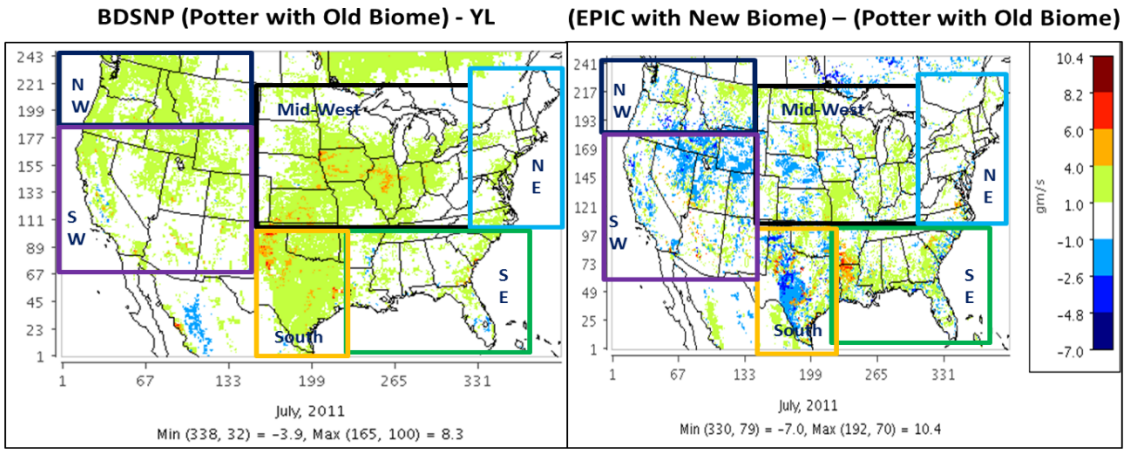

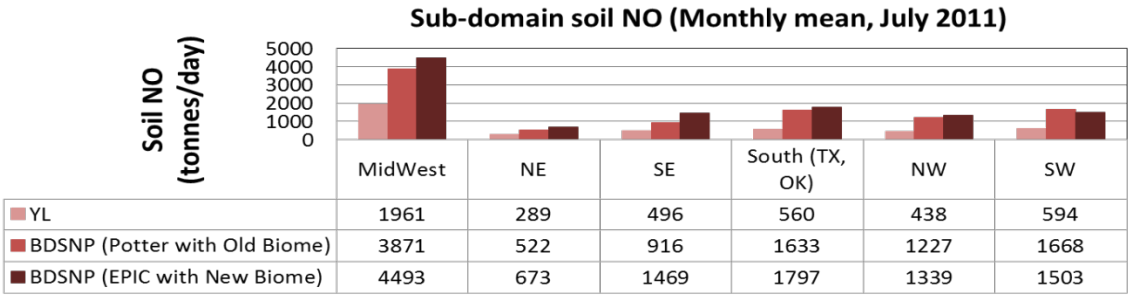

	MidWest	NE	SE	South (TX, OK)	NW	SW
YL	1961	289	496	560	438	594
BDSNP (Potter with Old Biome)	3871	522	916	1633	1227	1668
BDSNP (EPIC with New Biome)	4493	673	1469	1797	1339	1503

Figure 6 Soil NO (tonnes/day) sensitivity to change from YL to BDSNP (Potter and old biome or 'old') (left) and to the fertilizer and biome scheme within BDSNP (right) over sub-domains (boxes).

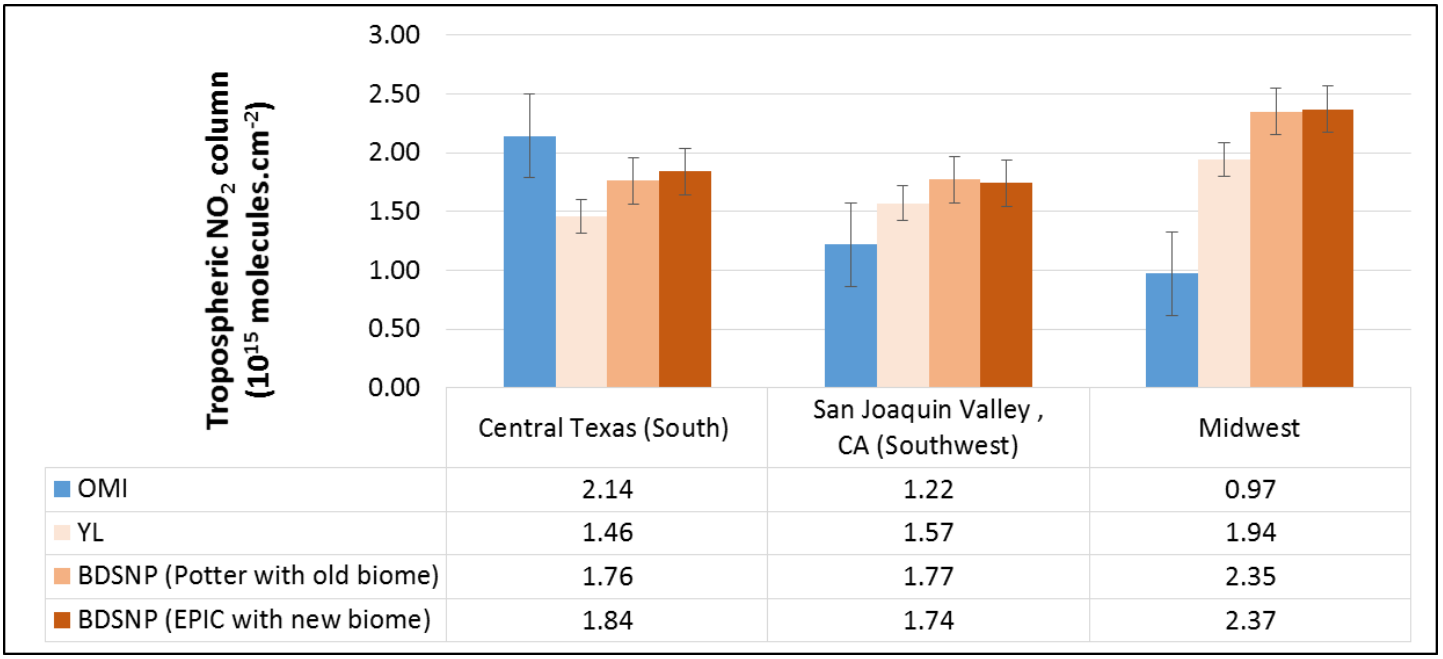

	Central Texas (South)	San Joaquin Valley , CA (Southwest)	Midwest
OMI	2.14	1.22	0.97
YL	1.46	1.57	1.94
BDSNP (Potter with old biome)	1.76	1.77	2.35
BDSNP (EPIC with new biome)	1.84	1.74	2.37

Figure 7 Spatial average for Tropospheric NO_2 (molecules cm^{-2}) over regions with high soil NO sensitivity with switch from YL to BDSNP (as in Figure 6) with comparison to OMI NO_2. NO_2 column are temporal average for July 2011 at OMI overpass time.

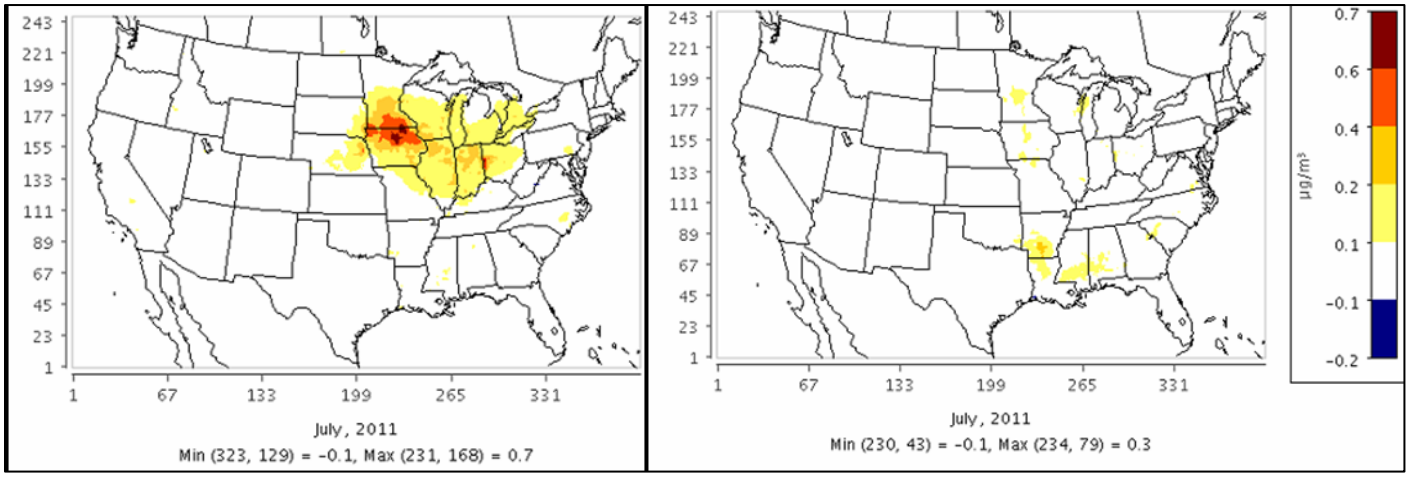

Figure 8 Changes in modeled daily average $PM_{2.5}$ when switching from: a) YL to BDSNP (Potter fertilizer data with original biome map) (left) and b) BDSNP (Potter with original biomes) to BDSNP (EPIC with new biomes) (right).

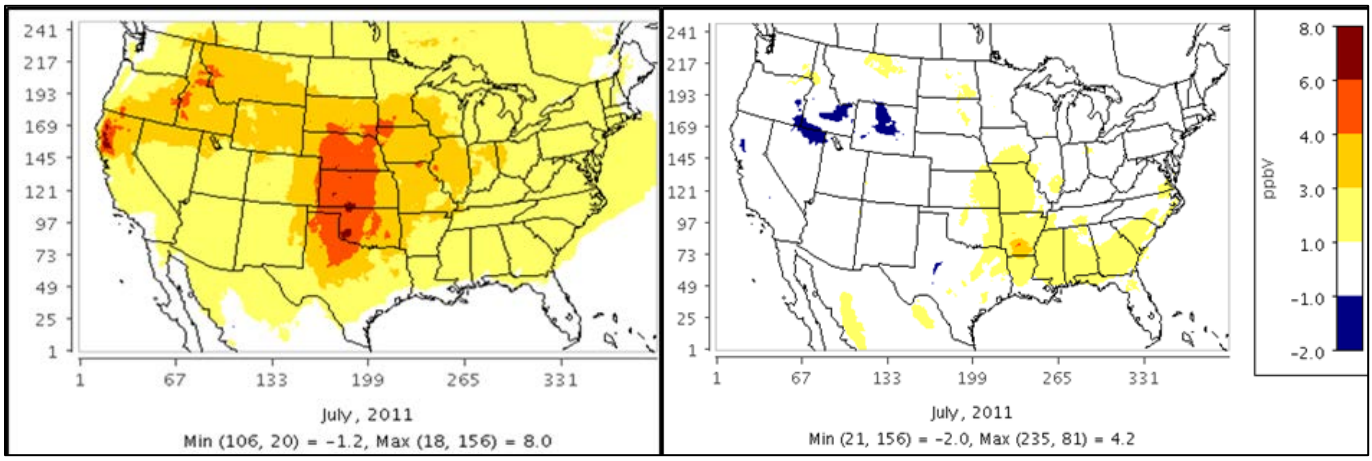

Figure 9 Changes in modeled maximum daily 8-hour ozone (MDA8) when switching from: a) YL to BDSNP (Potter fertilizer data with original biome map) (left) and b) BDSNP (Potter with original biomes) to BDSNP (EPIC with new biomes) (right).

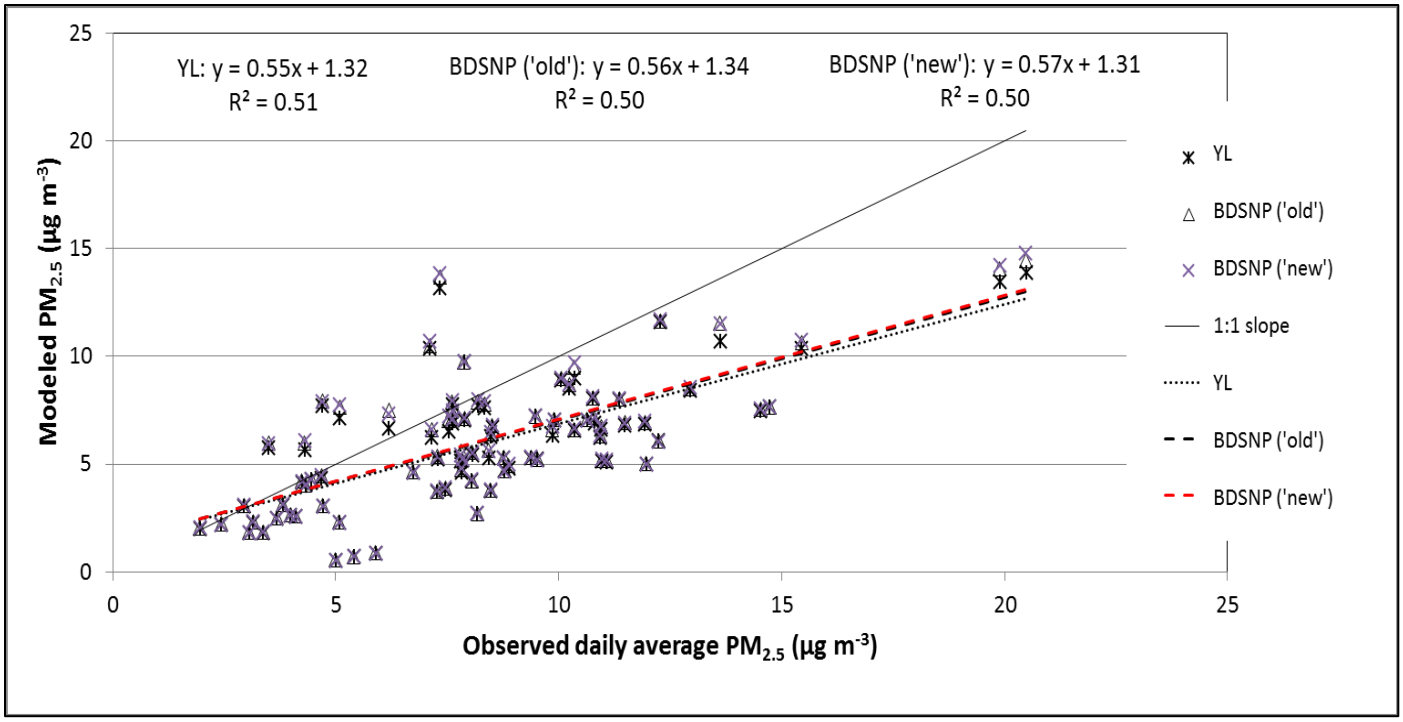

741

742

743

744 **Figure 10** Comparison of the three inline BDSNP-CMAQ cases with IMPROVE $PM_{2.5}$ data
745 (Malm et al., 1994) in continental US for Daily Average $PM_{2.5}$ for July 2011.

746

747

748

749

750

751

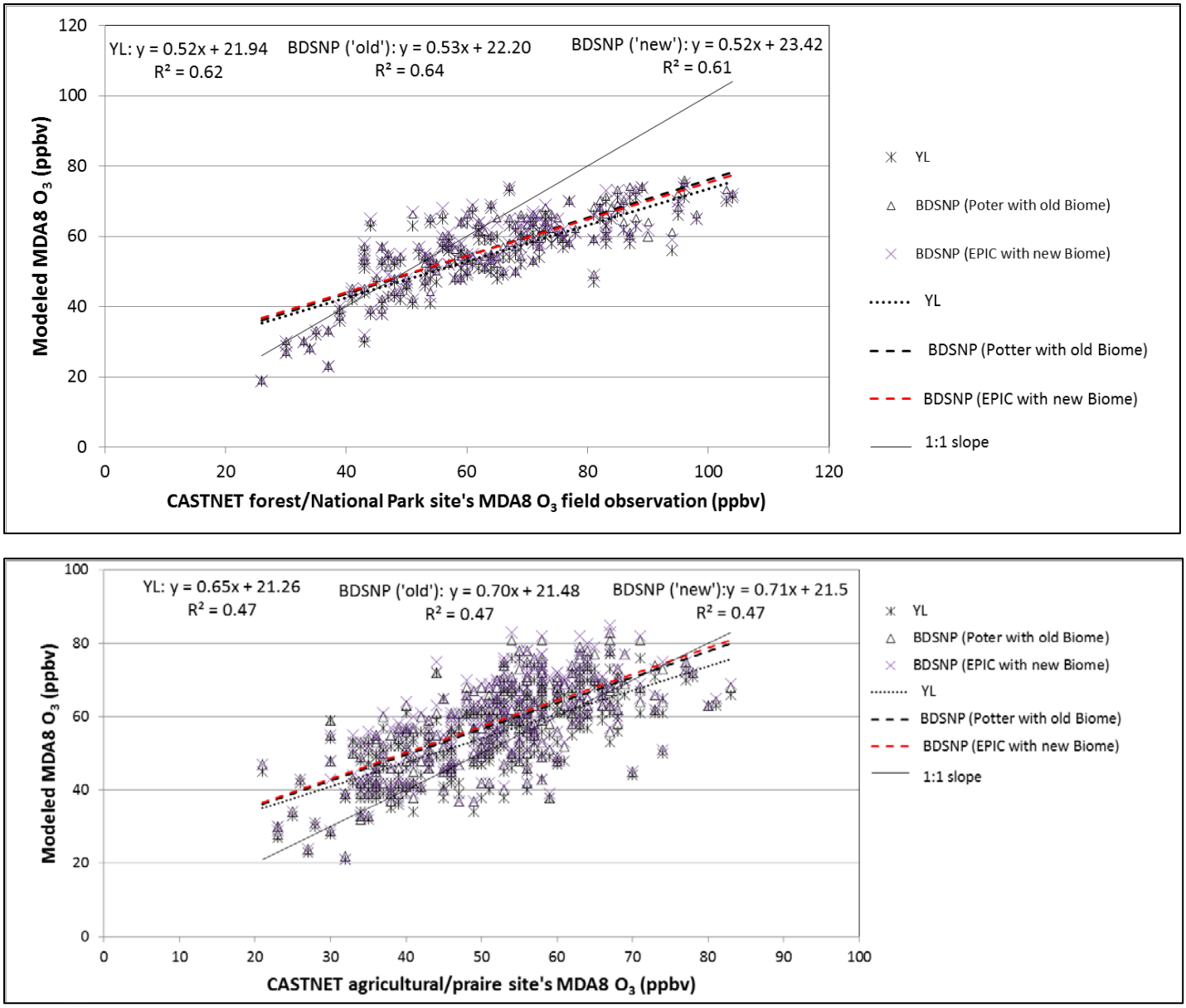

Figure 11 Comparison of the three inline BDSNP-CMAQ cases with CASTNET MDA8 O_3 data for forest/National Park sites in California (top, number of evaluation sites, n=147) and agricultural/prairie sites in mid-west and south US (bottom, n=311) for July 2011.

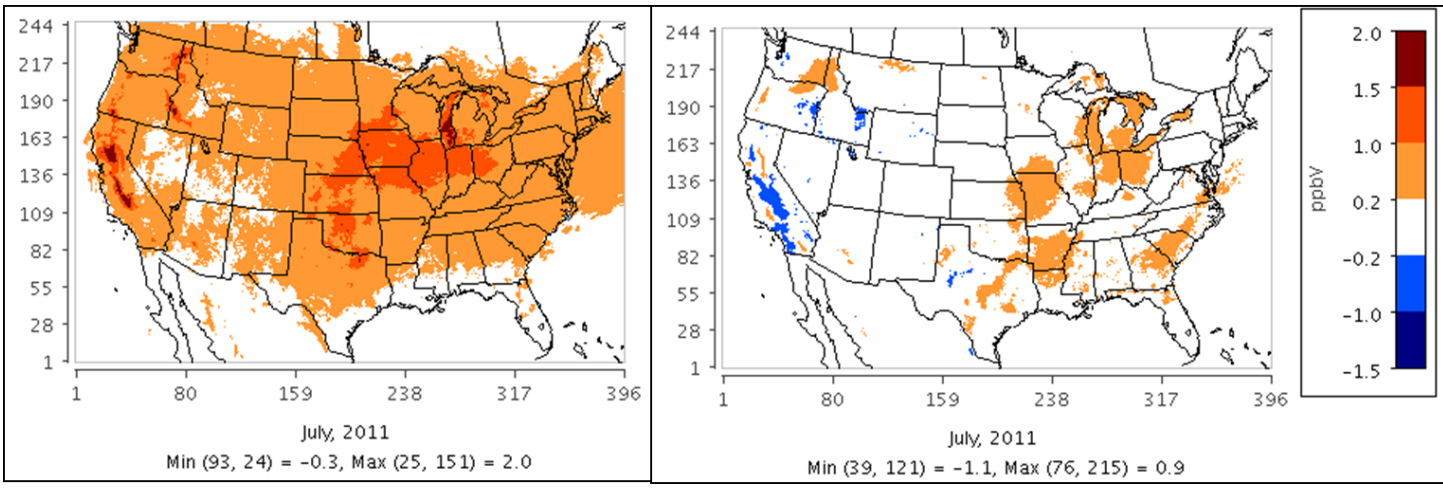

Figure 12 Difference in monthly mean MDA8 O_3 perturbation between: a) BDSNP ('old') – YL (left) and, b) BDSNP ('new') – BDSNP ('old') (right). MDA8 O_3 perturbations are from perturbed anthropogenic NO_x estimates 2011 base case to 2025 base case, BAU (US EPA, 2015).

777 **Table 1** Modeling configuration used for the WRF-BDSNP-CMAQ CONUS domain runs.

WRF/MCIP			
Version:	ARW V3.6.1	**Shortwave radiation:**	RRTMG scheme
Horizontal resolution:	CONUS (12kmX12km)	**Surface layer physic:**	Pleim-Xiu surface model
Vertical resolution:	26 layer	**PBL scheme:**	ACM2
Boundary condition:	NARR 32km	**Microphysics:**	Morrison double-moment scheme
Initial condition:	NCEP-ADP	**Cumulus parameterization:**	Kain-Fritsch scheme
Longwave radiation:	RRTMG scheme	**Assimilation:**	Analysis nudging above PBL for temperature, moisture and wind speed
BDSNP			
Horizontal resolution:	Same as WRF/MCIP	**Emission factor:**	Steinkamp and Lawrence (2011)
Soil Biome type:	24 types based on NLCD40 (new) 24 types based on GEOS-Chem LSM (old)	**Fertilizer database:**	EPIC 2011 based from FEST-C (new) Potter et al. (2010) (old)
CMAQ			
Version:	V5.02	**Anthropogenic emission:**	NEI2011
Horizontal resolution:	Same as WRF/MCIP	**Biogenic emission:**	BEIS V3.1 in-line
Initial condition:	Pleim-Xiu (new) GEOS-Chem (old)	**Boundary condition:**	Pleim-Xiu (new) GEOS-Chem (old)
Aerosol module:	AE5	**Gas-phase mechanism:**	CB-05
Simulation Case Arrangement (in-line with CMAQ)			
1. YL:	WRF/MCIP-CMAQ with standard YL soil NO scheme		
2. BDSNP (Potter with old Biome or 'old'):	WRF/MCIP-BDSNP-CMAQ with Potter and old biome		
3. BDSNP (EPIC with new Biome or 'new'):	WRF/MCIP-BDSNP-CMAQ with EPIC and new biome		
Simulation Time Period			
	July 1-31, 2011 for CMAQ simulation with **inline soil NO BDSNP module** Daily simulations in Year 2011 for **offline BDSNP** soil NO BDSNP module (July 1-31, 2011 for sensitivity analysis)		
Model Performance Evaluation			
USEPA Clean Air Status and Trends Network (CASTNET) data for MDA8 ozone Interagency Monitoring of Protected Visual Environments (IMPROVE) Network (Malm et al., 1994) for $PM_{2.5}$ OMI NO_2 satellite retrieval product as derived in Lamsal et al., 2014 for NO_2 column			

778

779 **Table 2** Aggregated performance statistics of CMAQ modeled daily average $PM_{2.5}$ for stations
780 showing sensitivities with change in soil NO between YL scheme and our 2 inline BDSNP
781 implementations ('old' and 'new') for CONUS in July 2011 as compared to observations at these
782 sites

Metrics				
	Sample Size		81	
	Mean observed ($\mu g/m^3$)		8.26	
	3 CMAQ inline cases	YL	BDSNP (Potter with old biome)	BDSNP (EPIC with new biome)
Daily average $PM_{2.5}$ July (1 July- 31 July), 2011	Mean predicted ($\mu g/m^3$)	5.91	6.04	6.08
	MAGE (Mean Absolute Gross error)	2.86	2.80	2.77
	RMSE	3.45	3.40	3.38
	R (correlation coefficient) Pearson's	0.72	0.71	0.71
	R (correlation coefficient) Spearman's Ranked	0.65	0.63	0.63
	NMB (%)	-28.52	-26.90	-26.44
	NME (%)	34.64	33.88	33.57

783

784

785

Table 3 Performance statistics of CMAQ modeled MDA8 Ozone for 16 CASTNET remote sites grouped into two categories: a) 11 sites with moist or wet soil condition (monthly mean soil moisture (m^3/m^3), $\theta_{mean} > 0.175$), and b) 5 sites with dry soil condition ($\theta_{mean} < 0.175$) , using soil NO from YL and our two inline BDSNP schemes.

July 2011	Metrics				
11 CASTNET sites (mostly agricultural/ prairie sites, Mostly wet soil conditions)	Sample size		311		
	Mean observed (ppbv)		51.76		
	3 CMAQ inline cases		YL	BDSNP (Potter with old biome)	BDSNP (EPIC with new biome)
	Mean modeled (ppbv)		55.25	57.93	58.60
	M_{AGE} (Mean Absolute Gross error)		7.78	9.16	9.65
	RMSE		9.41	10.96	11.47
	R (correlation coefficient)	Pearson's	0.50	0.51	0.50
		Spearman's Ranked	0.46	0.49	0.48
	NMB (%)		7.57	12.80	14.08
	NME (%)		15.65	18.38	19.33
5 CASTNET sites (mostly forest/National Park sites near San Joaquin valley CA, Dry soil conditions)	Sample size		147		
	Mean observed (ppbv)		64.38		
	Mean modeled (ppbv)		55.17	57.01	56.87
	M_{AGE} (Mean Absolute Gross error)		11.41	10.13	10.44
	RMSE		13.13	11.80	12.12
	R (correlation coefficient)	Pearson's	0.71	0.72	0.72
		Spearman's Ranked	0.68	0.69	0.69
	NMB (%)		-13.14	-10.23	-10.35
	NME (%)		16.95	15.04	15.45

Table 4 Emission perturbation factors applied to anthropogenic NO_x emissions for each sector listed in NEI as per EPA's RIA base-line reductions from 2011 to 2025 with BAU (Table 2A-1, https://www3.epa.gov/ttn/ecas/docs/20151001ria.pdf)

Sectors (NEI file names)	Perturbation factor
Electric Generating Unit(EGU)-point (ptimp- ptegu, ptegu_pk)	0.7
NonEGU-point (ptnonipm)	1
Point oil and gas (pt_oilgas)	0.92
Nonpoint oil and gas (np_oilgas)	1.108
Wild and Prescribed Fires (ptwildfire, ptprescfire)	1
Residential wood combustion (rwc)	1.029
Other nonpoint (nonpt)	1.039
Onroad (onroad)	0.298
Nonroad mobile equipment sources (nonroad)	0.5
Category 3 Commercial marine vessel (c3marine)	0.77
Locomotive and Category 1/Category 2 Commercial marine vessel (c1c2rail)	0.62

Appendix

Table A1 List of 24 soil biome emission factor (EF) from Steinkamp and Lawrence (2011)

ID	MODIS land cover	Köppen main climate(1)	EF1 (world geometric mean)	EF2 (world arithmetic mean)	EF3 (North American)
1	Water	--	0	0	0
2	Permanent wetland	--	0	0	0
3	Snow and ice	--	0	0	0
4	Barren	D,E	0	0	0
5	Unclassified	--	0	0	0
6	Barren	A,B,C	0.06	0.06	0.06
7	Closed shrub land	--	0.09	0.21	0.05
8	Open shrub land	A,B,C	0.09	0.21	0.09
9	Open shrub land	D,E	0.01	0.01	0.01
10	Grassland	D,E	0.84	1.05	0.62
11	Savannah	D,E	0.84	1.05	0.84
12	Savannah	A,B,C	0.24	0.97	0.24
13	Grassland	A,B,C	0.42	1.78	0.37
14	Woody savannah	--	0.62	0.74	0.62
15	Mixed forest	--	0.03	0.14	0.00
16	Evergreen broadleaf forest	C,D,E	0.36	0.95	0.36
17	Deciduous broadleaf forest	C,D,E	0.36	0.95	0.61
18	Deciduous needle. forest	--	0.35	0.95	0.35
19	Evergreen needle. forest	--	1.66	4.60	1.66
20	Deciduous. broadl. forest	A,B	0.08	0.13	0.08
21	Evergreen broadl. forest	A,B	0.44	1.14	0.44
22	Cropland	--	0.57	3.13	0.33
23	Urban and build-up lands	--	0.57	3.13	0.57
24	Cropland/nat. veg. mosaic	--	0.57	3.14	0.57

(1). A-equatorial, B-arid, C-warm temperature, D-snow, E-polar (see Figure 2 for spatial map)

806 **Table A2** Mapping table to create the 'new' soil biome map based on NLCD40 MODIS land
807 cover categories

ID	NLCD40 MODIS CATEGORY (40)	ID	SOIL BIOME CATEGORY (24)
1	Evergreen Needle leaf Forest	19	Evergreen Needle leaf Forest
2	Evergreen Broadleaf Forest	16 and 21	Evergreen Broadleaf Forest
3	Deciduous Needle leaf Forest	18	Dec. Needle leaf Forest
4	Deciduous Broadleaf Forest	17 and 20	Dec. Broadleaf Forest
5	Mixed Forests	15	Mixed Forest
6	Closed shrublands	7	Closed shrublands
7	Open shrublands	8 and 9	Open srublands
8	Woody Savannas	14	Woody savannah
9	Savannas	11 and 12	Savannah
10	Grasslands	10 and 13	Grassland
11	Permanent Wetlands	2	Permanent Wetland
12	Croplands	22	Cropland
13	Urban and Built Up	23	Urban and build-up lands
14	Cropland-Natural Vegetation Mosaic	24	Cropland/nat. veg. mosaic
15	Permanent Snow and Ice	3	Snow and ice
16	Barren or Sparsely Vegetated	6	Barren
17	IGBP Water	1	Water
18	Unclassified	1	Water
19	Fill value	1	Water
20	Open Water	1	Water
21	Perennial Ice-Snow	3	Snow and ice
22	Developed Open Space	23	Urban and build-up lands
23	Developed Low Intensity	23	Urban and build-up lands
24	Developed Medium Intensity	23	Urban and build-up lands
25	Developed High Intensity	23	Urban and build-up lands
26	Barren Land (Rock-Sand-Clay)	24	Cropland/nat. veg. mosaic
27	Unconsolidated Shore	24	Cropland/nat. veg. mosaic
28	Deciduous Forest	16 and 21	Evergreen Broadleaf Forest
29	Evergreen Forest	19	Evergreen Needle leaf Forest
30	Mixed Forest	15	Mixed Forest
31	Dwarf Scrub	8 and 9	Open shrublands
32	Shrub-Scrub	8 and 9	Open shrubland
33	Grassland-Herbaceous	10 and 13	Grassland
34	Sedge-Herbaceous	14	Woody savannah
35	Lichens	10 and 13	Grassland
36	Moss	10 and 13	Grassland
37	Pasture-Hay	24	Cropland/nat. veg. mosaic
38	Cultivated Crops	22	Cropland
39	Woody Wetlands	2	Permanent Wetland
40	Emergent Herbaceous Wetlands	2	Permanent Wetland

808

809 **Table A3** Summary of differences between YL, and the two applications of BDSNP. See Table
810 1 for other aspects of model configuration.

	Features	YL	BDSNP (Potter with old biome)	BDSNP (EPIC with new biome)
1)	NO emission response to biome, temperature and moisture	YL scheme uses a much generalized biome classification by grouping 36 NASA Global Vegetation Indexes to 11 broad biome types. Ice, desert and snow are attributed zero NO emission. The rest of biomes use emission factors that are empirical function of soil temperature behaving differently for dry and wet soils. Linear variation with soil temperature for dry soil, exponential response to temperature for wet soils (Yienger and Levy, 1995).	Biome emission factors for 40 NLCD land use categories, based on a coarse grid definition from GEOS-Chem LSM (Hudman et al., 2012). Non-linear response to soil temperature (T) and moisture (θ).	Biome emission factors regrouped from NLCD 40 to 24 MODIS land use types (Steinkamp and Lawrence, 2011) with Köppen climate definitions (Kottek et al., 2006) to be consistent with finer grid resolution used by Pleim-Xiu LSM in CMAQ. Non-linear response to soil T and θ.
2)	NO emission response to deposition	Deposition not accounted for as a source of soil N.	Deposition accounted for as a soil N source, but separately from fertilizer.	Deposition accounted for as a soil N source. FEST-C soil N Deposition (oxidized and reduced) outputs used, also includes bi-directional exchange capability of CMAQ, currently implemented for NH_3 (reduced N deposition source) only (Bash et al., 2013).
3)	NO emission response to Fertilizer	Considers planting date and a decline from NO fertilizer over the course of the growing season.	Potter et al. (2010) long-term average fertilizer estimates used.	Daily fertilizer estimates from EPIC/FEST-C, accounting for meteorology and farm practices (Cooter et al. 2012).

811

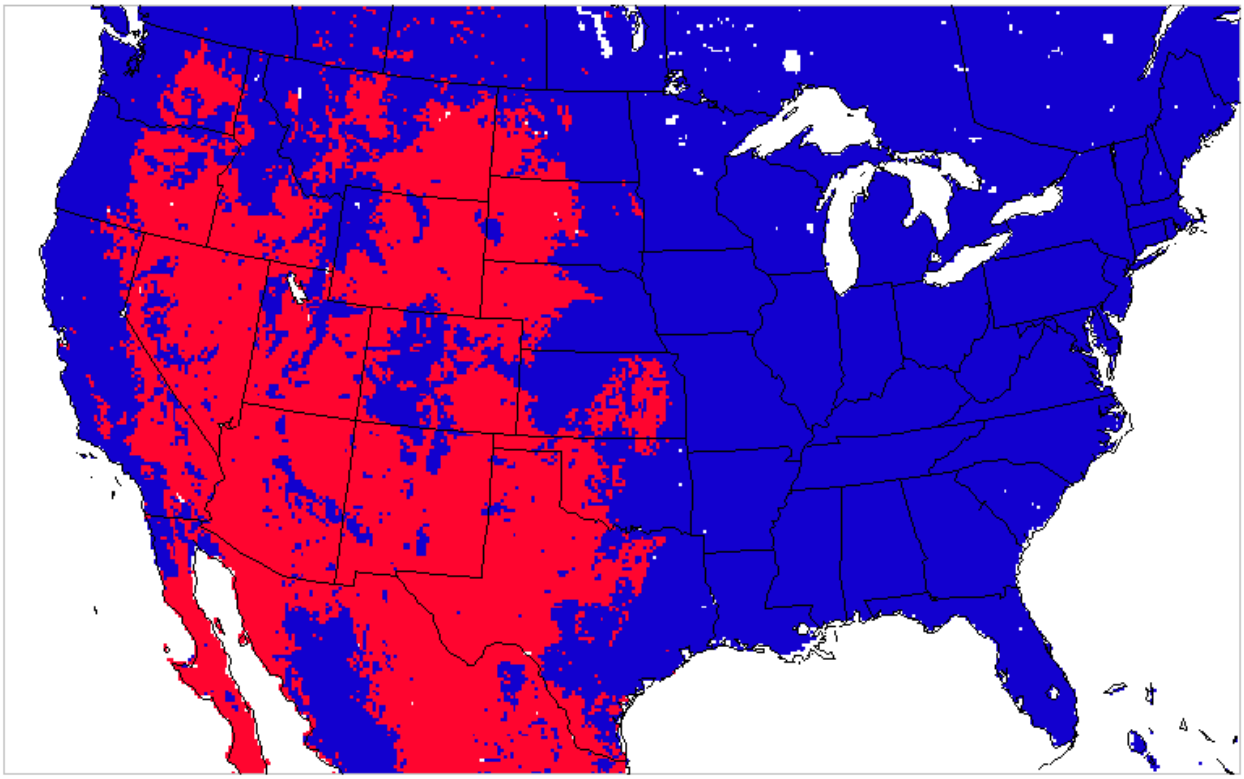

Figure B1 Arid (red) and non-arid (blue) region over Continental US (12km resolution)

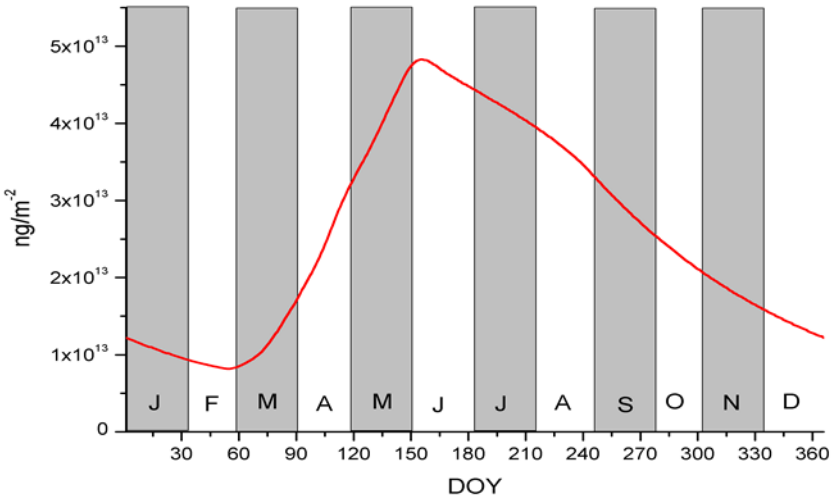

Figure B2 Daily variation of total N from fertilizer application (from Potter et al. (2010)) processed from BDSNP to establish timing over continental US throughout 2011

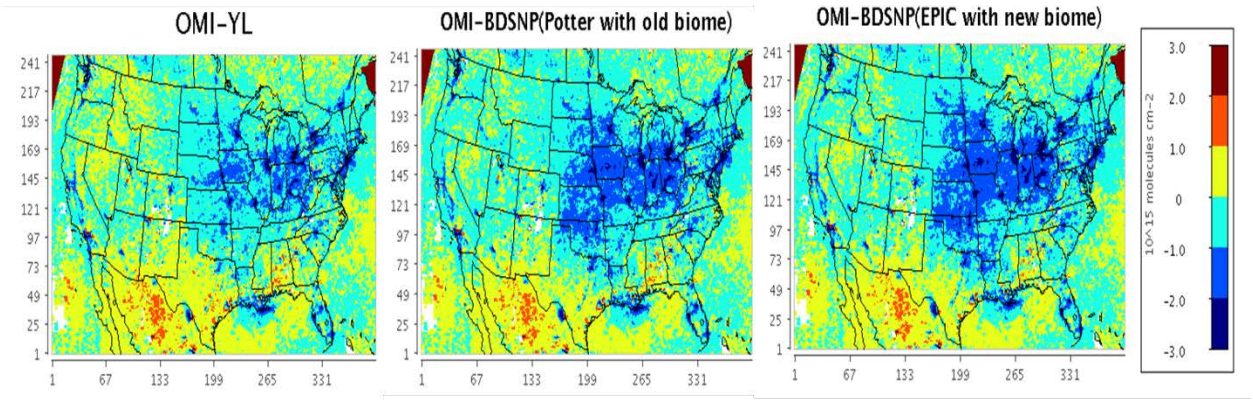

819

820 **Figure B3** Difference of OMI NO_2 column with NO_2 column simulated from the three inline
821 CMAQ cases: YL, BDSNP (Potter with old biome), BDSNP (EPIC with new Biome) (left to
822 right) over OMI overpass time averaged for July 2011 over CONUS. Note: In contour plots,
823 white refers to gaps/no-fill values in OMI product and dark red at upper corners are due to gaps
824 in CMAQ NO_2 column after temporal averaging at OMI overpass time.